

Gaussian process regression with log-linear scaling for common non-stationary kernels

P. Michael Kielstra¹ and Michael Lindsey^{1,2}

¹*University of California, Berkeley*

²*Lawrence Berkeley National Laboratory*

March 28, 2025

Abstract

We introduce a fast algorithm for Gaussian process regression in low dimensions, applicable to a widely-used family of non-stationary kernels. The non-stationarity of these kernels is induced by arbitrary spatially-varying vertical and horizontal scales. In particular, any stationary kernel can be accommodated as a special case, and we focus especially on the generalization of the standard Matérn kernel. Our subroutine for kernel matrix-vector multiplications scales almost optimally as $O(N \log N)$, where N is the number of regression points. Like the recently developed equispaced Fourier Gaussian process (EFGP) methodology, which is applicable only to stationary kernels, our approach exploits non-uniform fast Fourier transforms (NUFFT). We offer a complete analysis controlling the approximation error of our method, and we validate the method's practical performance with numerical experiments. In particular we demonstrate improved scalability compared to state-of-the-art rank-structured approaches in spatial dimension $d > 1$.

1 Introduction

Gaussian Process Regression (GPR) is widely used across many scientific fields [5, 13, 15, 17, 22, 36] as a framework for inferring a function $f : \mathbb{R}^d \rightarrow \mathbb{R}$ from noisy observations at an arbitrary collection of scattered points $x_1, \dots, x_N \in \mathbb{R}^d$. The success of GPR owes to its convenient linear-algebraic algorithmic formulation and its capacity for interpretable uncertainty quantification.

GPR is based on the selection of a prior distribution over functions, induced by a choice of positive definite kernel [36] $\mathcal{K}(x, y)$ defined for $x, y \in \mathbb{R}^d$. The key operations of GPR can be phrased linear-algebraically in terms of the kernel matrix $\mathbf{K} = (K(x_i, x_j))_{i,j=1}^N$. In particular, assuming a noise model in which the observations $y_n = f(x_n) + \epsilon_n$ are perturbed from the true values by independent and identically distributed Gaussian noise terms $\epsilon_n \sim \mathcal{N}(0, \eta^2)$, the key algorithmic step in GPR is the solution of the linear system

$$(\mathbf{K} + \eta^2 I_N) \alpha = y, \quad (1.1)$$

where $y = (y_1, \dots, y_N)^\top$ is the vector of observations. In turn the mean of the posterior distribution over functions, given the observations, can be recovered [36] from the solution vector α as

$$\mu(x) = \sum_{n=1}^N \alpha_n \mathcal{K}(x, x_n). \quad (1.2)$$

Uncertainty of this estimator can be quantified using the covariance function of the posterior, which can also be written linear-algebraically [36] as

$$\Sigma(x, y) = \mathcal{K}(x, y) - \mathcal{K}(x, x_m) \left[(\mathbf{K} + \eta^2 I_N)^{-1} \right]_{mn} \mathcal{K}(x_n, y). \quad (1.3)$$

A key task in GPR is therefore is to perform linear solves involving the matrix $\mathbf{K} + \eta^2 I$. Naively, forming the matrix requires $\Omega(N^2)$ operations, and direct solvers require $\Omega(N^3)$ operations. Since the matrix is positive definite, the conjugate gradient (CG) method [43] can be applied using the dense matrix to potentially reduce the overall cost to $\Omega(N^2)$, assuming a condition number independent of N , and parallelism may be exploited to further improve the practical scaling [45].

Our focus is on approaches with faster than quadratic scaling, which requires the exploitation of some sort of structure of \mathbf{K} . In particular, we hope for the nearly-optimal scaling of $\tilde{O}(N)$, where \tilde{O} indicates the omission of logarithmic factors. Though we will review a few paradigms for fast GPR, we refer the reader to [20] for an excellent summary of the literature.

The most straightforward paradigms include low-rank factorization of \mathbf{K} [31, 36] and sparse thresholding of \mathbf{K} [16]. However, there exist many scenarios in which neither the numerical rank nor sparseness suffice for tractable computations. When the spatial dimension d is low, more sophisticated structured rank decompositions have emerged as a paradigm for the compression of \mathbf{K} . These decompositions can also permit direct algorithms for the required linear solves. Structured formats used for GPR include the hierarchically off-diagonal low-rank (HODLR) format, as well as the HSS and HBS formats [1, 26, 23, 25]. Such approaches are extremely effective in $d = 1$, but their performance can noticeably degrade even for $d = 2$ as the relevant numerical ranks can grow with both d and N .

Greengard et al. [20] recently introduced a method for kernel matrix-vector multiplications (or matvecs) with $\tilde{O}(N)$ cost that eschews both sparse and low-rank compression entirely. Their equispaced Fourier Gaussian process (EFGP) approach relies on non-uniform fast Fourier transforms (NUFFT) [9, 14]. A detailed analysis controlling the error of EFGP is explored in [2]. However, a major limitation of this approach is the assumption that the kernel is *stationary*, i.e., satisfies $\mathcal{K}(x, y) = \mathcal{K}(x - y)$.

In our own language, the idea of [20] can be summarized as follows. Suppose that we wish to compute an arbitrary matvec $\mathbf{K}\alpha$. Observe the identity:

$$[\mathbf{K}\alpha]_m = \left[\mathcal{K} \sum_{n=1}^N \alpha_n \delta_{x_n} \right] (x_m),$$

where we view \mathcal{K} as an integral operator with kernel $\mathcal{K}(x, y)$ and let δ_x denote the Dirac delta distribution localized at x . Then letting \mathcal{F} denote the unitary Fourier transform (and \mathcal{F}^* its inverse), we have equivalently that

$$[\mathbf{K}\alpha]_m = \left[\mathcal{F}^* \hat{\mathcal{K}} f \right] (x_m), \text{ where } f := \mathcal{F} \sum_{n=1}^N \alpha_n \delta_{x_n}, \quad (1.4)$$

and $\hat{\mathcal{K}} := \mathcal{F}\hat{\mathcal{K}}\mathcal{F}^*$. Since \mathcal{K} is stationary, it follows that $\hat{\mathcal{K}}$ is a diagonal operator. Meanwhile, f as defined in (1.4) can be computed on a grid in Fourier space using a type 1 NUFFT (cf. Appendix D for further background). Once $\hat{\mathcal{K}}f$ is formed on the Fourier grid, then the entries of $\mathbf{K}\alpha$ can be recovered via (1.4) using a type 2 NUFFT (again refer to Appendix D). The total cost is $O(M^d + N \log N)$, where M is the number of discretization points per dimension in Fourier space. Viewing M as a constant controlling the error of the method, the matvec scaling is $O(N \log N)$ as desired.

Our work aims to extend the success of EFGP to the commonly used family of *non-stationary kernels* (especially, non-stationary, *Matérn* kernels), developed in [32, 34] and recently applied in contemporary settings requiring flexible kernel design [28, 29]. Settings in which the non-stationary Matérn kernel has been shown to be well-adapted include IR and neutron spectroscopy [30] and climatology [33]. Even without non-stationary capabilities, the classical Matérn kernel has been successfully applied in fields ranging from astronomy and astrophysics [21, 6] to nanofluid modeling [27] and chemical engineering [35].

Our strategy is made up of several intermediate steps that allow us to reduce, like [20], to diagonal operations on a Fourier grid, though the operations that we require are different. First, we exploit the ‘Schoenberg’ representation (cf. [37, Theorem 2] as well as (2.2) below) of the positive definite function that induces the non-stationary kernel [34], to essentially reduce to the case of non-stationary squared exponential kernels. In fact, this Schoenberg representation is fundamental to the derivation [34] of the non-stationary kernel family of interest. Second, we use interpolation by value of the non-stationary scale function $\sigma(x)$ that defines our non-stationary kernel (cf. (2.3) below) to reduce the application of the kernel to the task of applying several Gaussian convolutions, which can be achieved as diagonal operations in Fourier space. Like [20], we require NUFFTs of both type 1 and type 2 to pass from the scattered grid to the equispaced Fourier grid and vice versa.

We prove exponential convergence of our approximation with respect to all hyperparameters of the algorithm that control the error. In terms of the target error ϵ as well as the Matérn parameter ν , cf. (2.4), the computational complexity of the approach is $O(\epsilon^{-dp})$ where d is the spatial dimension and p is any exponent larger than $(2\nu)^{-1}$. The scaling is due to the necessity of constructing a Fourier grid with ϵ^{-p} points per dimension. For a rigorous statement and further detail, see Theorem 14 and the discussion that immediately follows it. Interestingly, even in the special case of a stationary kernel, our analysis differs from that of [20] due to the substitution of the Schoenberg representation of the kernel, which we discretize (cf. Section 3.2 and Lemma 4 below) with rapidly-converging numerical quadrature. Although passing through the Schoenberg representation is apparently a forced move in our analysis, due to the structure of our non-stationary kernel family, ultimately our error analysis yields almost the same complexity as that of [20] for stationary Matérn kernels, where a Fourier grid with $O(\epsilon^{-1/(2\nu)})$ points per dimension is likewise constructed.

We demonstrate the effectiveness of our method with several numerical experiments, and in particular we compare our results to the highly performant FLAM package [23] which is based on hierarchical low-rank decompositions.

As in [20], we do not discuss preconditioning. Potentially, our method for kernel matvecs could be combined with a preconditioner based on a low-accuracy hierarchical decomposition. We highlight this direction, as well as other approaches for preconditioning, as interesting topics for future research.

1.1 Outline

In Section 2 we present the family of non-stationary kernels that are of interest in this work. In Section 3 we discuss our approximation framework for this kernel, which is based on (1) quadrature for the Schoenberg representation, (2) interpolation by value of the scale function, and (3) Fourier space discretization. This framework motivates the explicit algorithm presented in Section 4. We outline our error analysis in Section 5 and present relevant numerical experiments and benchmarks in Section 6.

We provide a glossary of some of our key notation in Appendix A and review some background on NUFFT in Appendix D. The remaining appendices give more details on proofs that we defer in the main body of the paper: the general integral representation of the kernel in Appendix B, the construction of an explicit Schoenberg representation for the Matérn kernel specifically in Appendix C, and the various technical components of our error bound in Appendix E. The lemmas are synthesized in Appendix F, the proof of our main theorem on the error bound.

1.2 Acknowledgments

This work was partially supported by the Applied Mathematics Program of the US Department of Energy (DOE) Office of Advanced Scientific Computing Research under contract number DE-AC02-05CH11231 (M.L.).

2 Preliminaries

A rich family of non-stationary kernels, introduced in [32, 34], is specified by the general functional form

$$\mathcal{K}(x, y) = w(x) w(y) |\Sigma(x) + \Sigma(y)|^{-1/2} \varphi \left(\sqrt{(x - y)^\top [\Sigma(x) + \Sigma(y)]^{-1} (x - y)} \right), \quad (2.1)$$

where $\Sigma(x) \succ 0$ is an arbitrary $d \times d$ positive-definite-matrix-valued function of the spatial variable $x \in \mathbb{R}^d$, $w(x) \geq 0$ is an arbitrary nonnegative-valued function, vertical bars indicate the matrix determinant, and $\varphi : [0, \infty) \rightarrow \mathbb{R}$ is an arbitrary *radial positive definite* function, meaning that

$$\Phi(x) = \varphi(\|x\|)$$

is a positive definite function in the sense of [38].

It is known by a theorem of Schoenberg [37, Theorem 2] that φ is radial positive definite if and only if it can be written as

$$\varphi(r) = \int_0^\infty e^{-r^2 s^2} d\mu(s), \quad (2.2)$$

where μ is a finite nonnegative Borel measure on $[0, \infty)$. This characterization motivates the intuitive understanding of the family (2.1) as being generated by nonnegative linear combinations of ‘non-stationary squared exponential kernels’ of the form

$$\mathcal{K}(x, y) = w(x) w(y) |\Sigma(x) + \Sigma(y)|^{-1/2} e^{-\frac{1}{2}(x-y)^\top [\Sigma(x) + \Sigma(y)]^{-1} (x-y)}.$$

The Gaussian processes induced by such kernels are themselves derived [34] by smoothing a white noise process with a Gaussian windowing function with spatially dependent covariance. More generally, representing a function as an integral over a family of Gaussians, to be approximated with a discrete sum, is a common technique; see, for example, [7] and [8].

In this work, we focus on the important special case of *non-stationary isotropic kernels*, in which the structure of $\Sigma(x)$ simplifies as

$$\Sigma(x) = \sigma^2(x) I_d, \quad (2.3)$$

where $\sigma(x) > 0$ is scalar-valued. By a linear change of the spatial variable, it is easy to reduce to this case from the more general case

$$\Sigma(x) = \sigma^2(x) \Sigma_0,$$

where Σ_0 is an arbitrary $d \times d$ positive semidefinite matrix, independent of x .

With regard to the selection of φ , of particular interest is the case of non-stationary Matérn kernels [34], induced by the choice $\varphi = \varphi_\nu$:

$$\varphi_\nu(r) = \frac{1}{2^{\nu-1}\Gamma(\nu)} \left| \sqrt{2\nu} r \right|^\nu K_\nu \left(\sqrt{2\nu} r \right), \quad (2.4)$$

where $\nu > 0$ is a fixed parameter that governs the smoothness of kernel and K_ν is the modified Bessel function of the second kind. (Everywhere, the letter K is reserved for kernel-related quantities; we use it for the Bessel function only here.)

In general, a function drawn from a GP specified by a Matérn kernel with $\nu > 0$ will be continuous and $\lceil \nu \rceil - 1$ times differentiable [36, Section 4.2]. In practice, the typically chosen values of ν are the half-integers $\frac{1}{2}, \frac{3}{2}, \frac{5}{2} \dots$, since for these values, the Bessel function K_ν admits a closed-form expression that can be easily evaluated. Since we deal with φ_ν only via its Schoenberg representation (2.2), which we explicitly construct in Appendix B, there is no reason to favor half-integer ν in our implementation, though the cost of our algorithm will increase without bound in the $\nu \rightarrow 0$ limit. We remark that $\nu = \frac{1}{2}$ is the lowest value that appears in common practice, corresponding to the case $\varphi(r) \propto e^{-r}$ of the exponential kernel. Meanwhile, in the $\nu \rightarrow \infty$ limit, we recover [36, Section 4.2] the squared exponential kernel function

$$\varphi(r) = e^{-\frac{r^2}{2}}, \quad (2.5)$$

which is of special interest.

3 Approximation of the kernel

A general non-stationary isotropic kernel in the sense of Section 2 (cf. (2.3)) can be written

$$\mathcal{K}(x, y) = w(x) w(y) \left(2\pi [\sigma^2(x) + \sigma^2(y)] \right)^{-d/2} \varphi \left(\frac{|x - y|}{\sqrt{\sigma^2(x) + \sigma^2(y)}} \right), \quad (3.1)$$

where $\sigma(x) > 0$ and $w(x) \geq 0$ are arbitrary. We will assume upper and lower bounds σ_{\max} and $\sigma_{\min} > 0$ such that

$$\sigma(x) \in [\sigma_{\min}, \sigma_{\max}]$$

for all $x \in \mathbb{R}^d$. As we shall see, the ratio

$$\kappa := \frac{\sigma_{\max}}{\sigma_{\min}} \quad (3.2)$$

will in part control the numerical difficulty of representing such a non-stationary isotropic kernel.

Note that, without any loss of generality, we have absorbed a factor into the weight function $w(x)$ in order to ease certain manipulations downstream in the discussion.

In order to approximate the integral kernel \mathcal{K} in a framework that will permit fast kernel matrix-vector multiplications, we will adopt the following strategy. First we represent the function $\varphi(r)$ as an integral over a family of Gaussians parametrized by a variable t . Then, we discretize the integral, which essentially reduces the treatment of \mathcal{K} to the case where φ is Gaussian in (3.1). In order to remove the non-stationarity in (3.1) due to the spatial dependence of $\sigma(x)$, we approximate $\sigma(x)$ with Chebyshev interpolation. This step allows us to approximate any Gaussian integral kernel with spatially-varying standard deviation as a weighted sum of stationary Gaussian convolutions. To apply the integral operator \mathcal{K} , these reductions leave us with a batch of what are now explicitly Gaussian convolutions, which we can compute cheaply using NUFFTs.

3.1 Analytical integration in t

Let us suppose for simplicity that φ is induced in (2.2) by an absolutely continuous measure μ , as is the case in all important applications that we shall highlight below. Then it is possible to write

$$\varphi(r) = \int e^{-\frac{r^2}{2\chi^2(t)}} u(t) dt \quad (3.3)$$

for suitable functions $\chi : \mathbb{R} \rightarrow (0, \infty)$ and $u : \mathbb{R} \rightarrow [0, \infty)$. In fact, such a representation is non-unique via change of variables, but later we shall consider explicit representations that allow for convenient numerical discretization of the integral dt .

In this case, the kernel (3.1) is recovered exactly by the representation

$$\mathcal{K} = \int_{\mathbb{R}} \mathcal{B}_t \mathcal{B}_t^* v(t) dt, \quad (3.4)$$

where each \mathcal{B}_t (for $t \in \mathbb{R}$) is an integral kernel defined by

$$\mathcal{B}_t(x, z) = w(x) [2\pi \sigma^2(x)]^{-d/2} e^{-\frac{|x-z|^2}{2\sigma(x)^2 \chi(t)^2}}, \quad (3.5)$$

and moreover

$$v(t) := \chi^{-d}(t) u(t), \quad (3.6)$$

as we verify in Appendix B. Note that we view \mathcal{B}_t as both an integral operator as well as a function $\mathbb{R}^d \times \mathbb{R}^d \rightarrow \mathbb{R}$ defining the integral kernel of this operator. We will maintain calligraphic notation for such objects, including \mathcal{K} as well.

In particular, we compute (cf. (B.1)) that

$$(\mathcal{B}_t \mathcal{B}_t^*)(x, y) v(t) = w(x) w(y) (2\pi [\sigma^2(x) + \sigma^2(y)])^{-d/2} e^{-\frac{|x-y|^2}{2(\sigma(x)^2 + \sigma(y)^2) \chi(t)^2}} u(t). \quad (3.7)$$

Meanwhile, as we prove in Appendix C, the Matérn function (2.4) is recovered exactly by the choice

$$u(t) := \frac{1}{\Gamma(\nu)} e^{\nu t - e^t}, \quad \chi(t) := \frac{1}{\sqrt{\nu}} e^{t/2}. \quad (3.8)$$

In the special case of the squared exponential kernel (2.5), there is no real need for integration in t . We can formally take $u(t) = \delta(t)$ and $\chi^2(t) \equiv 1$ in (3.3) to recover this case.

3.2 Numerical integration in t

We now discuss how to discretize the integral with respect to t in the integral representation (3.4) of the kernel, in the Matérn case (3.8).

In fact, we shall approximate the integral with a simple trapezoidal Riemann sum:

$$\mathcal{K} \approx \sum_{j=0}^{N_t} \mathcal{B}_{t_j} \mathcal{B}_{t_j}^* v_j, \quad (3.9)$$

where

$$v_j = \begin{cases} v(t_j) \Delta t, & j \in \{1, \dots, N_t - 1\}, \\ v(t_j) \frac{\Delta t}{2}, & j \in \{0, N_t\}. \end{cases}$$

Since the dependence on t of $(\mathcal{B}_t \mathcal{B}_t^*)(x, y) v(t)$ in (3.7) is analytic with exponentially decaying tails, we can effectively restrict to a compact domain of integration, and moreover we expect rapid convergence [44] as Δt is refined. The error due to this discretization will be controlled explicitly in Lemma 4 below.

Specifically, after choosing $t_{\min} < t_{\max}$ bounding the effective interval of integration and a number of integration points $N_t + 1$, we set $\Delta t = \frac{t_{\max} - t_{\min}}{N_t}$ and

$$t_j = t_{\min} + \frac{j}{N_t} (t_{\max} - t_{\min}), \quad j = 0, \dots, N_t. \quad (3.10)$$

In the special case of the squared exponential kernel (2.5), there is no need to approximate the integral in t . We can recover this case by taking $N_t = 0$, $t_{\min} = t_{\max} = 0$, and $v_0 = 1$, as well as $\chi^2(0) = 1$, as indicated above.

3.3 Chebyshev interpolation in σ

Each operator \mathcal{B}_t can be viewed as the composition $\mathcal{B}_t = \mathcal{D}_t \mathcal{C}_t$ of the diagonal multiplier

$$\mathcal{D}_t(x, z) = w(x) [2\pi \sigma^2(x)]^{-d/2} \delta(x - z) \quad (3.11)$$

with the integral operator

$$\mathcal{C}_t(x, z) := e^{-\frac{|x-z|^2}{2\sigma^2(x)\chi^2(t)}}. \quad (3.12)$$

From a computational point of view, dealing with \mathcal{C}_t is difficult because it is not precisely a convolution operator, due to the non-stationary dependence $\sigma(x)$. Therefore we are motivated to replace

\mathcal{C}_t with a linear combination of operators which are themselves true convolution operators, and we achieve this by Chebyshev interpolation with respect to the *value* of $\sigma(x)$.

To wit, let

$$\sigma_k = \frac{\cos(\pi k/N_\sigma) + 1}{2} (\sigma_{\max} - \sigma_{\min}) + \sigma_{\min}, \quad k = 0, \dots, N_\sigma, \quad (3.13)$$

denote the Chebyshev-Lobatto grid with $N_\sigma + 1$ points on the interval $[\sigma_{\min}, \sigma_{\max}]$. Let P_k be the Lagrange interpolating polynomials for this grid, i.e., the polynomials of degree N_σ such that $P_k(\sigma_j) = \delta_{jk}$.

Then we approximate $\mathcal{C}_t(x, z)$ via Chebyshev interpolation as

$$\mathcal{C}_t^{(N_\sigma)}(x, z) := \sum_{k=0}^{N_\sigma} P_k(\sigma(x)) \mathcal{G}_{k,t}(x, z), \quad (3.14)$$

in which each term

$$\mathcal{G}_{k,t}(x, z) := e^{-\frac{|x-z|^2}{2\sigma_k^2 \chi^2(t)}} \quad (3.15)$$

is a *bona fide* Gaussian convolution operator.

In turn we may define

$$\mathcal{B}_t^{(N_\sigma)} := \mathcal{D}_t \mathcal{C}_t^{(N_\sigma)}, \quad (3.16)$$

which approximates \mathcal{B}_t . By lumping together the diagonal multiplier \mathcal{D}_t (3.11) with the diagonal multiplier $P_k(\sigma(x))$, we may define a diagonal operator

$$\mathcal{W}_k(x, z) := \underbrace{w(x) [2\pi \sigma^2(x)]^{-d/2} P_k(\sigma(x))}_{=: w_k(x)} \delta(x - z) \quad (3.17)$$

such that

$$\mathcal{B}_t^{(N_\sigma)} = \sum_{k=0}^{N_\sigma} \mathcal{W}_k \mathcal{G}_{k,t}. \quad (3.18)$$

3.4 Fourier discretization

The preceding discussion motivates us to perform fast computation with the operator $\mathcal{B}_t^{(N_\sigma)} \mathcal{B}_t^{(N_\sigma)*}$. However, the internal ‘ dz ’ integration implicit in the product of these two integral operators must be discretized. This discretization will be achieved by choosing a grid in Fourier space. One motivation for considering a Fourier discretization is that the convolution operations introduced above can naturally be performed as pointwise multiplications in Fourier space.

In the following, we let \mathcal{F} denote the unitary Fourier transform on \mathbb{R}^d . Then we approximate

$$\mathcal{B}_t^{(N_\sigma)} \mathcal{B}_t^{(N_\sigma)*} \approx \mathcal{B}_t^{(N_\sigma)} \mathcal{F}^* \Pi^* \Pi \mathcal{F} \mathcal{B}_t^{(N_\sigma)*} (\Delta\omega)^d,$$

where $\Pi = \Pi^{(M, \Delta\omega)}$ acts by restricting its input to a discrete grid defined in terms of two parameters, M and $\Delta\omega$. Concretely, the restriction $\Pi \hat{f}$ of a function \hat{f} to the grid can be viewed as a function of $\mathbf{n} \in \{-M, \dots, M\}^d$ obtained as $(\Pi \hat{f})[\mathbf{n}] = \hat{f}(\mathbf{n} \Delta\omega)$. We will typically omit the dependence of Π on M and $\Delta\omega$ from the notation to avoid notational clutter.

Note that the formal adjoint Π^* acts on grid functions $a = a[\mathbf{n}]$ via

$$\Pi^* a = \sum_{\mathbf{n} \in \{-M, \dots, M\}^d} a[\mathbf{n}] \delta_{\mathbf{n} \Delta \omega},$$

with equality in the sense of distributions, so that

$$\Pi^* \Pi \hat{f} = \sum_{\mathbf{n} \in \{-M, \dots, M\}^d} \hat{f}(\mathbf{n} \Delta \omega) \delta_{\mathbf{n} \Delta \omega}.$$

3.5 Summary

In summary, we propose to approximate the kernel \mathcal{K} (3.1) as

$$\tilde{\mathcal{K}} := \sum_{j=0}^{N_t} \tilde{v}_j \mathcal{B}_{t_j}^{(N_\sigma)} \mathcal{F}^* \Pi^* \Pi \mathcal{F} \mathcal{B}_{t_j}^{(N_\sigma)*}, \quad (3.19)$$

in which expression we now define

$$\tilde{v}_j := (\Delta \omega)^d v_j$$

to simplify our notation.

In total, the hyperparameters that must be chosen to define this approximation are t_{\min}, t_{\max}, N_t (for numerical integration in t , cf. Section 3.2 above), N_σ (for interpolation in σ , cf. Section 3.3 above), and $M, \Delta \omega$ (for Fourier discretization, cf. Section 3.4 above). We will analyze the error as a function of these choices in Section 5 below. Before doing so, we will derive in Section 4 a fast algorithm for kernel matrix-vector multiplication using the approximation $\tilde{\mathcal{K}}$.

4 Fast algorithm for kernel matrix-vector multiplication

For arbitrary scattered points $x_1, \dots, x_N \in \mathbb{R}^d$, define the $N \times N$ kernel matrix

$$\mathbf{K} = (\mathcal{K}(x_i, x_j))_{i,j=1}^N. \quad (4.1)$$

Our goal is to perform the matrix-vector multiplication $\mathbf{K}\alpha$ with nearly-linear scaling in N , the size of the dataset, where $\alpha = (\alpha_j) \in \mathbb{R}^N$ is an arbitrary vector.

To approximate this result, we may likewise define

$$\tilde{\mathbf{K}} = \left(\tilde{\mathcal{K}}(x_i, x_j) \right)_{i,j=1}^N, \quad (4.2)$$

where $\tilde{\mathcal{K}}$ is defined as in (3.19) and the dependence on our approximation hyperparameters is again omitted for notational clarity. We will explain how to compute $\tilde{\mathbf{K}}\alpha$ *exactly* (ignoring only, for simplicity, the numerical error in the application of various NUFFT's). Note that the positive semidefiniteness of the approximate kernel matrix $\tilde{\mathbf{K}}$ is automatically guaranteed from the representation (3.19) of $\tilde{\mathcal{K}}$.

Our derivation will involve first rewriting (3.19) so that the convolutions by individual Gaussians take place in Fourier space. We will then order the sums over our discrete values of σ and t to optimize the implementation. This will give us an expression for $\tilde{\mathbf{K}}\alpha$ from which we can simply read off our algorithm by applying its constituent operators from right to left.

4.1 Derivation

For fixed α , define the distribution

$$f := \sum_{i=1}^N \alpha_i \delta_{x_i}.$$

The first step is to realize that

$$\left[\tilde{\mathbf{K}}\alpha \right]_i = (\tilde{\mathcal{K}}f)(x_i). \quad (4.3)$$

Now, inserting (3.18) into our representation (3.19) of $\tilde{\mathcal{K}}$, we expand:

$$\tilde{\mathcal{K}}f = \sum_{k'=0}^{N_\sigma} \mathcal{W}_{k'} \sum_{j=0}^{N_t} \tilde{v}_j \mathcal{G}_{k',t_j} \mathcal{F}^* \Pi^* \sum_{k=0}^{N_\sigma} \Pi \mathcal{F} \mathcal{G}_{k,t_j} \mathcal{W}_k f. \quad (4.4)$$

We will insert resolutions of the identity $\mathcal{F}\mathcal{F}^* = \text{Id}$ and $\mathcal{F}^*\mathcal{F} = \text{Id}$ into (4.4) to obtain

$$\tilde{\mathcal{K}}f = \sum_{k'=0}^{N_\sigma} \mathcal{W}_{k'} \sum_{j=0}^{N_t} \tilde{v}_j \mathcal{F}^* \hat{\mathcal{G}}_{k',t_j} \Pi^* \sum_{k=0}^{N_\sigma} \Pi \hat{\mathcal{G}}_{k,t_j} \mathcal{F} \mathcal{W}_k f, \quad (4.5)$$

where

$$\hat{\mathcal{G}}_{k,t} := \mathcal{F} \mathcal{G}_{k,t} \mathcal{F}^*$$

is the Fourier-space representation of the Gaussian convolution operator, i.e., a diagonal multiplier by a suitable Gaussian. We will also define

$$\hat{G}_{k,t} := \Pi \hat{\mathcal{G}}_{k,t} \Pi^*$$

denote the suitable restriction of $\mathcal{G}_{k,t}$ to a diagonal multiplier on our $(M, \Delta\omega)$ -Fourier grid. Note that in fact

$$\Pi \hat{\mathcal{G}}_{k,t} = \hat{G}_{k,t} \Pi, \quad \hat{\mathcal{G}}_{k,t} \Pi^* = \Pi^* \hat{G}_{k,t}$$

from which facts, together with (4.5), it follows that

$$\tilde{\mathcal{K}}f = \sum_{k'=0}^{N_\sigma} \mathcal{W}_{k'} [\mathcal{F} \Pi]^* \sum_{j=0}^{N_t} \tilde{v}_j \hat{G}_{k',t_j} \sum_{k=0}^{N_\sigma} \hat{G}_{k,t_j} \underbrace{\Pi \mathcal{F} [\mathcal{W}_k f]}_{\text{type 1 NUFFT}}. \quad (4.6)$$

Observe that the underbraced expression, which is a function on the Fourier grid, can be constructed exactly as the type 1 NUFFT (cf. Appendix D, and recall from (3.17) the definition of the diagonal multiplier \mathcal{W}_k) of the vector $c_k \in \mathbb{R}^N$ of values

$$c_{k,i} := w_k(x_i) \alpha_i, \quad (4.7)$$

associated to the scattered points $\{x_i\}_{i=1}^N$.

Using results of these $(N_\sigma + 1)$ type 1 NUFFTs, we can form the Fourier grid function $a_k = a_k[\mathbf{n}]$ indicated with the overbrace in (4.6) by a sequence of pointwise multiplications and summations.

Given the result a_k , we now indicate the computation that remains for determining $\left[\tilde{\mathbf{K}}\alpha\right]_i$, following 4.3:

$$\left[\tilde{\mathbf{K}}\alpha\right]_i = (\tilde{\mathcal{K}}f)(x_i) = \sum_{k=0}^{N_\sigma} w_k(x_i) \underbrace{([\mathcal{F}\Pi]^* a_k)(x_i)}_{\text{type 2 NUFFT}}. \quad (4.8)$$

Observe that the collection of values $\{([\mathcal{F}\Pi]^* a_k)(x_i)\}_{i=1}^N$ indicated with the underbrace can be recovered precisely as the type 2 NUFFT (cf. Appendix D) of the Fourier grid function a_k , evaluated on the scattered points $\{x_i\}_{i=1}^N$.

4.2 Explicit algorithm and cost scaling

We concretely summarize the algorithmic steps indicated above in the discussion of (4.6) and (4.8).

- (1) For each $k = 0, \dots, N_\sigma$, form the vector $c_k \in \mathbb{R}^N$, following (4.7).
 - **Cost scaling:** $O(N_\sigma N)$.
- (2) For each $k = 0, \dots, N_\sigma$, form the Fourier grid function $b_k = b_k[\mathbf{n}]$ as the type 1 NUFFT of c_k on the scattered points $\{x_i\}_{i=1}^N$. (These $(N_\sigma + 1)$ type 1 NUFFTs can be batched in parallel.)
 - **Cost scaling:** $O(N_\sigma M^d + N_\sigma N \log N)$, cf. Appendix D.
- (3) For each $k' = 0, \dots, N_\sigma$, form $a_{k'} := \sum_{j=0}^{N_t} \tilde{v}_j \hat{G}_{k', t_j} \sum_{k=0}^{N_\sigma} \hat{G}_{k, t_j} b_k$.
 - **Cost scaling:** $O(M^d N_\sigma \min(N_\sigma, N_t))$, cf. Remark 1 below for further detail.
- (4) For each $k = 0, \dots, N_\sigma$, form $\beta_k \in \mathbb{R}^N$ as the type 2 NUFFT of the the Fourier grid function a_k , evaluated on the scattered points $\{x_i\}_{i=1}^N$. (These $(N_\sigma + 1)$ NUFFTs can also be batched.)
 - **Cost scaling:** $O(N_\sigma M^d + N_\sigma N \log N)$, cf. Appendix D.
- (5) Then $\tilde{\mathbf{K}}\alpha$ is finally recovered as $\sum_{k=0}^{N_\sigma} w_k(x_i) \beta_k$.
 - **Cost scaling:** $O(N_\sigma N)$. Note that $w_k(x_i)$ can be precomputed in step 1.

Remark 1. Note that performing step 3 directly requires us to perform one matrix-vector multiplication of size $(N_t + 1) \times (N_\sigma + 1)$ and another of size $(N_\sigma + 1) \times (N_t + 1)$, for each point on the Fourier grid. In total the cost scaling of this approach amounts to $O(M^d N_\sigma N_t)$.

Alternatively, we may precompute the tensor

$$A_{k', k}[\mathbf{n}] = \sum_{j=0}^{N_t} \tilde{v}_j \hat{G}_{k', t_j}[\mathbf{n}, \mathbf{n}] \hat{G}_{k, t_j}[\mathbf{n}, \mathbf{n}]$$

with offline cost $O(M^d N_\sigma^2 N_t)$. Then once this tensor is formed, we may form the Fourier grid functions $a_{k'}$ in terms of the b_k as

$$a_{k'}[\mathbf{n}] = A_{k', k}[\mathbf{n}] b_k[\mathbf{n}]$$

with online cost $O(M^d N_\sigma^2)$. This is useful when $(N_t + 1) \geq (N_\sigma + 1)/2$ since we need to perform only a single matrix-vector multiplication of size $(N_\sigma + 1) \times (N_\sigma + 1)$ for each Fourier grid point.

Even when N_σ becomes large, we comment that precomputation may still be useful if it is possible to factorize each $A_{k',k}[\mathbf{n}] \approx \sum_{\alpha=1}^r R_{k'}^\alpha[\mathbf{n}] R_k^\alpha[\mathbf{n}]$ in low-rank form. This could allow the user to set N_t very large, oversampling the integral in t , and then reveal the rank that is empirically required, rather than fixing it a priori. We leave further investigation of this point to future work.

In summary, the total cost scaling of a matvec is

$$O(N_\sigma N \log N + M^d N_\sigma \min(N_\sigma, N_t)), \quad (4.9)$$

though refer to Remark 1 for a discussion of a potential offline cost.

We comment that the fast Gauss transform (FGT) [18, 40, 19] might also be used to accelerate the applications of $\mathcal{G}_{k,t}$. However, we would have to run one FGT for each of the $O(N_t N_\sigma)$ Gaussians by which wish to convolve. Since the FGT cost scales linearly in the number of input points, an FGT-based algorithm would have an $O(N_t N_\sigma N)$ term in its cost-scaling expression.

5 Error analysis

In Section 4, we presented a fast algorithm for matrix-vector multiplication by the approximate kernel matrix $\tilde{\mathbf{K}}$ (4.2). In this section, we want to bound the error compared to multiplication by the true kernel matrix \mathbf{K} (4.2)

We will accomplish this by bounding the error $\|\mathcal{K} - \tilde{\mathcal{K}}\|$ in a suitable norm $\|\cdot\|$, which in turn controls the error $\|\mathbf{K} - \tilde{\mathbf{K}}\|_p$ for any operator p -norm. We bound the norm $\|\mathcal{K} - \tilde{\mathcal{K}}\|$ in three stages:

- (1) bounding the error due to numerical integration in t , cf. Section 3.2 above,
- (2) bounding the error due to interpolation in σ , cf. Section 3.3 above, and
- (3) bounding the error due to Fourier discretization, cf. Section 3.4 above.

For simplicity we will assume that our scattered points $\{x_i\}_{i=1}^N$ are contained in the bounding box $[-1, 1]^d$. This assumption does not lose any generality, as we can reduce to this scenario by shifting and scaling the problem.

Now observe that for any $\alpha \in \mathbb{R}^N$ and any $p \in [1, \infty]$

$$\|\mathbf{K}\alpha - \tilde{\mathbf{K}}\alpha\|_p \leq \|\mathbf{K} - \tilde{\mathbf{K}}\|_p \|\alpha\|_p,$$

where $\|\cdot\|_p$ denotes the ℓ^p vector norm as well as the corresponding operator norm. In fact, it will be most convenient to bound the error $\mathbf{K} - \tilde{\mathbf{K}}$ in the ‘uniform entrywise’ norm, which is not an operator norm.

Definition 2. For an $N \times N$ matrix A , we define

$$\|A\| = \max_{i,j \in \{1, \dots, N\}} |A_{ij}|.$$

Likewise, for an integral kernel $A(x, y)$ which is a continuous function of (x, y) , we define (overloading notation slightly) the analogous norm

$$\|A\| := \sup_{x, y \in [-1, 1]^d} |A(x, y)|.$$

Fortunately, the uniform entrywise norm on matrices controls all p -operator norms as follows:

Lemma 3. *For any $N \times N$ matrix A and any $p \in [1, \infty]$, we have $\|A\|_p \leq N \|A\|$.*

The proof is given in Appendix E for completeness, since this fact is not too frequently encountered.

Following Lemma 3, as well as the immediate fact that $\|\mathbf{K} - \tilde{\mathbf{K}}\| \leq \|\mathcal{K} - \tilde{\mathcal{K}}\|$, the error of our kernel matrix-vector multiplication algorithm can be bounded as

$$\|\mathbf{K}\alpha - \tilde{\mathbf{K}}\alpha\|_p \leq N \|\mathcal{K} - \tilde{\mathcal{K}}\|$$

for any $p \in [1, \infty]$.

Thus, as indicated above, we are motivated to bound $\|\mathcal{K} - \tilde{\mathcal{K}}\|$. For simplicity we will assume that

$$|w(x)| \leq 1, \text{ for all } x \in [-1, 1]^d. \quad (5.1)$$

Evidently, the entrywise norm $\|\mathcal{K} - \tilde{\mathcal{K}}\|$ scales more generally with an additional factor of $\|w\|_\infty^2$ where $\|w\|_\infty$ indicates the L^∞ norm on the bounding box. We reduce to the case $\|w\|_\infty \leq 1$ to avoid notational clutter.

In our error analysis we will view t_{\min} , t_{\max} , N_t , N_σ , M , and $\Delta\omega$ as the adjustable parameters, cf. the summary of these choices in Section 3.5. Meanwhile the dimension d and the Matérn parameter ν (2.4) will be viewed as constant from the point of view of big- O notation. A glossary of commonly used notation in our analysis is provided in Appendix A.

5.1 Stage (1)

The following lemma constitutes stage (1), in which we bound the error introduced by discretizing the integral in t .

Lemma 4. *For the Matérn function representation with u and χ as in (3.8), the following bound holds for any choice of $\alpha > 0$ and $\delta \in (0, 1)$:*

$$\left\| \mathcal{K} - \sum_{j=0}^{N_t} \mathcal{B}_{t_j} \mathcal{B}_{t_j}^* v_j \right\| = O \left(\sigma_{\min}^{-d} \left[e^{-\alpha t_{\max}} + e^{\nu t_{\min}} + e^{-\frac{(1-\delta)\pi^2}{\Delta t}} \right] \right),$$

where $\Delta t = \frac{t_{\max} - t_{\min}}{N_t}$ is assumed to be $O(1)$.

The proof is given in Appendix E. In brief, the third term in the error bound appearing in the statement of the lemma is due to the approximation of the integral in t with an infinite Riemann sum from $t = -\infty$ to $t = \infty$. The first and second terms, meanwhile, are due to the truncation of the tails of this Riemann sum outside of $[t_{\min}, t_{\max}]$.

Motivated by the result of Lemma 4, we make the following definition.

Definition 5. For any $t_{\min}, t_{\max} \in \mathbb{R}$, $N_t \geq 1$, and $\nu, \alpha > 0$, $\delta \in (0, 1)$, define

$$\epsilon_{\text{trap}}^{\nu, \alpha, \delta}(t_{\min}, t_{\max}, N_t) := e^{-\alpha t_{\max}} + e^{\nu t_{\min}} + e^{-\frac{(1-\delta)\pi^2}{\Delta t}}.$$

Usually we omit the dependence on ν, α, δ (which we can take to be fixed), as well as on t_{\min}, t_{\max} , and N_t (our adjustable parameters) from the notation, simply writing ϵ_{trap} .

5.2 Stage (2)

To accomplish stage (2), bounding the error due to Chebyshev interpolation in σ , first we show that Chebyshev interpolation of the Gaussian function in the *width* parameter attains uniform accuracy that is controlled only by $\kappa = \frac{\sigma_{\max}}{\sigma_{\min}}$ and the number of interpolating widths N_σ .

Lemma 6. For all $x \in \mathbb{R}$,

$$\left| e^{-\frac{x^2}{2\sigma^2}} - \sum_{k=1}^{N_\sigma} P_k(\sigma) e^{-\frac{x^2}{2\sigma_k^2}} \right| \leq 2(\kappa - 1) \left(\frac{\kappa - 1}{\kappa + 1} \right)^{N_\sigma}.$$

The proof is given in Appendix E and makes use of standard error bounds for Chebyshev interpolation of analytic functions [42]. Motivated by the result of Lemma 6, we make the following definition.

Definition 7. For any $\kappa \geq 1$ and integer $N_\sigma \geq 1$, define

$$\epsilon_{\text{cheb}}(N_\sigma, \kappa) = 2(\kappa - 1) \left(\frac{\kappa - 1}{\kappa + 1} \right)^{N_\sigma}.$$

As before, we will typically omit the dependence on N_σ and κ from the notation, simply writing ϵ_{cheb} .

We also make a few more definitions that are necessary to state the bound that finishes stage (2).

Definition 8. Let $\rho_{\max} = \sigma_{\max} \chi_{\max}$ and $\rho_{\min} = \sigma_{\min} \chi_{\min}$, where $\chi_{\max} := \chi(t_{\max})$ and $\chi_{\min} := \chi(t_{\min})$. Furthermore, let $\lambda = \frac{\rho_{\max}}{\rho_{\min}} = \kappa \frac{\chi_{\max}}{\chi_{\min}}$.

Definition 9. Let Λ_{N_σ} denote the Lebesgue constant [42] for Chebyshev interpolation on the nodes σ_k , i.e.,

$$\Lambda_{N_\sigma} := \sup_{\sigma \in [\sigma_{\min}, \sigma_{\max}]} \left\{ \sum_{k=0}^{N_\sigma} |P_k(\sigma)| \right\}.$$

It is known [42, Theorem 15.2] that $\Lambda_{N_\sigma} = O(\log N_\sigma)$.

Then Lemma 6 allows us to prove the following bound, which controls the error incurred in the kernel by our Chebyshev interpolation procedure.

Lemma 10. The bound

$$\left\| \mathcal{B}_t \mathcal{B}_t^* - \mathcal{B}_t^{(N_\sigma)} \mathcal{B}_t^{(N_\sigma)*} \right\| = O(\Lambda_{N_\sigma} \rho_{\max}^d \epsilon_{\text{cheb}})$$

holds uniformly in $t \in [t_{\min}, t_{\max}]$.

The proof is given in Appendix E.

5.3 Stage (3)

Finally, to accomplish stage (3), we want to bound the error incurred by the ‘insertion’ of $(\Delta\omega)^d \mathcal{F}^* \Pi^* \Pi \mathcal{F}$ within the product $\mathcal{B}_t^{(N_\sigma)} \mathcal{B}_t^{(N_\sigma)*}$. A first step to achieving this bound is the following lemma.

Lemma 11. *The bound*

$$\|(\Delta\omega)^d \mathcal{G}_{k,t} \mathcal{F}^* \Pi^* \Pi \mathcal{F} \mathcal{G}_{l,t} - \mathcal{G}_{k,t} \mathcal{G}_{l,t}\| = O\left(\rho_{\max}^d \left[\lambda^d e^{-[2\pi\rho_{\min} M \Delta\omega]^2} + e^{-[\frac{1}{4\rho_{\max} \Delta\omega}]^2}\right]\right)$$

holds uniformly over $t \in [t_{\min}, t_{\max}]$ and $k, l \in \{0, \dots, N_\sigma\}$, provided $\Delta\omega \leq \frac{1}{8}$.

The proof is based on bounding the Riemann sum approximation of the integral of a Gaussian using Poisson summation, and it is very similar to Theorem 2 of [2], for example. See also [44]. For completeness, we prove the result from scratch in Appendix E.

Motivated by the result of Lemma 11, we make the following definition.

Definition 12. *In terms of our adjustable hyperparameters and their dependent quantities, define*

$$\epsilon_{\mathcal{F}} := \lambda^d e^{-[2\pi\rho_{\min} M \Delta\omega]^2} + e^{-[\frac{1}{4\rho_{\max} \Delta\omega}]^2},$$

where as above we omit the dependence on the parameters from our notation.

Then the desired bound for stage (3) follows:

Lemma 13. *The bound*

$$\|(\Delta\omega)^d \mathcal{B}_t^{(N_\sigma)} \mathcal{F}^* \Pi^* \Pi \mathcal{F} \mathcal{B}_t^{(N_\sigma)*} - \mathcal{B}_t^{(N_\sigma)} \mathcal{B}_t^{(N_\sigma)*}\| = O\left(N_\sigma^2 \kappa^d \left[\frac{\chi_{\max}}{\sigma_{\min}}\right]^d \epsilon_{\mathcal{F}}\right)$$

holds uniformly in $t \in [t_{\min}, t_{\max}]$.

The proof is given in Appendix E.

5.4 Synthesizing the bounds

Now we can synthesize stages (1), (2), and (3) of the error analysis into our main approximation theorem.

Theorem 14. *For the non-stationary isotropic kernel \mathcal{K} (3.1) of Matérn type (with parameter ν) and approximation $\tilde{\mathcal{K}}$ (3.19), the following bound holds:*

$$\|\mathcal{K} - \tilde{\mathcal{K}}\| = O\left(\sigma_{\min}^{-d} \epsilon_{\text{trap}} + \Lambda_{N_\sigma} \rho_{\max}^d \epsilon_{\text{cheb}} + N_\sigma^2 \kappa^d \left[\frac{\chi_{\max}}{\sigma_{\min}}\right]^d \epsilon_{\mathcal{F}}\right),$$

provided that $\Delta t = O(1)$, $\Delta\omega \leq \frac{1}{8}$. In the case of the squared-exponential kernel, the bound instead reads as

$$\|\mathcal{K} - \tilde{\mathcal{K}}\| = O\left(\Lambda_{N_\sigma} \rho_{\max}^d \epsilon_{\text{cheb}} + N_\sigma^2 \kappa^d \left[\frac{\chi_{\max}}{\sigma_{\min}}\right]^d \epsilon_{\mathcal{F}}\right).$$

The proof is given in Appendix F. Please refer to Definitions 5, 7, and 12 for the definitions of ϵ_{trap} , ϵ_{cheb} , and $\epsilon_{\mathcal{F}}$. For other quantities, the glossary of Appendix A may provide a helpful supplement to the above discussion.

Given a user-selected tolerance ϵ for the pointwise error $\|\mathcal{K} - \tilde{\mathcal{K}}\|$, Theorem 14 offers a guide for selecting the adjustable parameters t_{\min} , t_{\max} , N_t , N_σ , M , and $\Delta\omega$. Recall that the parameters fixed by the problem specification are d , ν , σ_{\min} , and σ_{\max} . The reader is referred to Appendix Appendix A for the glossary of notation. Since our analysis is written in terms of big- O notation, we cannot make explicit choices that will achieve an error of at most ϵ . Nonetheless, we can offer a practical perspective on the procedure for choosing the parameters in terms of ϵ . The discussion is only informal, and the reader is encouraged to refer to the rigorous statement of Theorem 14.

- (1) First we choose t_{\min} , t_{\max} , and N_t to control ϵ_{trap} so that the first term in Theorem 14 is bounded as $\sigma_{\min}^{-d} \epsilon_{\text{trap}} = O(\epsilon)$. Based on Definition 5, concretely we take

$$-t_{\min} = \nu^{-1} \log(1/\epsilon) + \nu^{-1} d \log(1/\sigma_{\min}),$$

Similarly, we take

$$t_{\max} = \alpha^{-1} \log(1/\epsilon) + \alpha^{-1} d \log(1/\sigma_{\min}) + c_\alpha,$$

where $\alpha \geq 1$ is arbitrary and c_α is universal other than its dependence on α . Then given t_{\min} and t_{\max} , we choose

$$N_t = (t_{\max} - t_{\min}) \log(1/\epsilon)$$

- Now that t_{\min} and t_{\max} are fixed, the quantities λ , χ_{\min} , χ_{\max} , ρ_{\min} , and ρ_{\max} are also fixed.
- (2) Then we choose N_σ to control ϵ_{cheb} so that the second term in Theorem 14 is bounded as $\Lambda_{N_\sigma} \rho_{\max}^d \epsilon_{\text{cheb}} \leq \epsilon$. Based on Definition 7, we take

$$N_\sigma = O(\kappa [\log(1/\epsilon) + \log(\sigma_{\max})]).$$

We comment that in the large κ and small ϵ limit, asymptotically we can take $N_\sigma \sim \kappa \log(1/\epsilon)$.

- (3) Finally, we choose M and $\Delta\omega$ to control $\epsilon_{\mathcal{F}}$ so that the third term in Theorem 14 is bounded as $N_\sigma^2 \kappa^d \left[\frac{\chi_{\max}}{\sigma_{\min}} \right]^d \epsilon_{\mathcal{F}} = O(\epsilon)$. Based on Definition 12, we take

$$(\Delta\omega)^{-1} = \rho_{\max} \sqrt{\log(1/\epsilon) + \dots}$$

where the omitted terms are $O(d [\log \kappa + \log(1/\sigma_{\min}) + \log \log(1/\epsilon) + \log_+(1/\nu)])$. Then in terms of $\Delta\omega$, we choose

$$M = \frac{(\Delta\omega)^{-1}}{\rho_{\min}} \sqrt{(1 + \nu^{-1}) \log(1/\epsilon) + \dots}$$

where the omitted terms are $O(d [\log \kappa + \log_+(1/\nu)])$.

With these choices, the error $\|\mathcal{K} - \tilde{\mathcal{K}}\|$ will be $O(\epsilon)$. With all else held constant, we may determine the computational complexity in terms of the error tolerance ϵ and Matérn parameter ν by taking $N_t = O((\nu^{-1} + \alpha^{-1}) \log^2(1/\epsilon))$, $N_\sigma = O(\log(1/\epsilon))$, and

$$M = \frac{\rho_{\max}}{\rho_{\min}} O\left(\sqrt{1 + \nu^{-1}} \log(1/\epsilon)\right).$$

After observing that $\rho_{\max}/\rho_{\min} = \kappa e^{\frac{1}{2}(t_{\max}-t_{\min})}$ and plugging in our choices for t_{\max} and t_{\min} , we see that we can take

$$M = O(\epsilon^{-p})$$

where p is any exponent larger than $(2\nu)^{-1}$. By substituting into (4.9), we recover the final complexity $O(\epsilon^{-dp})$ for any such p . In particular, note that the requirements on the resolution of the Fourier grid become milder in the limit $\nu \rightarrow \infty$ of a smoother Matérn prior. In Section 6 below, we will numerically explore the effect of the tunable parameters on the accuracy of kernel matrix-vector multiplications.

6 Numerical experiments

Finally we present several numerical experiments validating the accuracy and performance of our approach. In Section 6.1 we explore the impact of our tunable parameters on the error control of an isolated kernel matvec. In Section 6.2 we wrap our matvec algorithm with a CG solver to solve a GPR problem and compare the scaling against the FLAM package [23]. All experiments were performed on a laptop with a 12th-generation Intel Core i7.

Throughout, we define a tolerance $\epsilon_{\text{NUFFT}} = 10^{-6}$ and take NUFFTs with a relative error tolerance of $\epsilon_{\text{NUFFT}}/10$. For a given maximum standard deviation ρ_{\max} , we will take $\Delta\omega = \min\left\{\frac{1}{8}, \frac{1}{4}\rho_{\max}^{-1}\log^{-1/2}(1/\epsilon_{\text{NUFFT}})\right\}$, which guarantees in particular (cf. Definition 12) that $e^{-\left[\frac{1}{4\rho_{\max}\Delta\omega}\right]^2} \leq \epsilon_{\text{NUFFT}}$. All relative errors for vectors are measured in the 2-norm.

In all experiments, the points x_i , $i = 1, \dots, N$, are chosen independently from the uniform distribution on $[-1, 1]^d$. We also fix $w(x) = 1$ and $\sigma(x) = \frac{1}{6}\left(\prod_{i=1}^d \cos(\pi x_i) + 2\right)$, except where otherwise indicated.

Code for all of our experiments is available at [24].

6.1 Matvecs

In this section we focus on the accuracy and cost of the computation of a single matvec $\mathbf{K}\alpha$.

First we fix the Matérn parameter $\nu = \frac{3}{2}$ and set $t_{\min} = (1 + \log \epsilon_{\text{NUFFT}})/\nu$ and $t_{\max} = \log(-2 \log \epsilon_{\text{NUFFT}})$. These values are chosen to be sufficiently small and large, respectively, such that they do not bottleneck the error in our experiments. From these choices we obtain $\chi_{\min} = \frac{1}{\sqrt{\nu}}e^{t_{\min}/2}$ and $\chi_{\max} = \frac{1}{\sqrt{\nu}}e^{t_{\max}/2}$. We also choose $\sigma_{\min} = \frac{1}{6} - 0.01$ and $\sigma_{\max} = \frac{1}{6} + 0.01$, in turn fixing the values of ρ_{\min} and ρ_{\max} .

Throughout all our experiments, we maintain this value of $\kappa = \sigma_{\max}/\sigma_{\min} \approx 3$. In practice, κ can vary widely: in a large geographical model, correlation lengths might vary from a few miles to a few hundred miles, yielding $\kappa \approx 100$ or even larger [30]. In general, κ will depend on the range of length scales present within the model.

Our tunable parameters are then N_t , N_σ , and M . We perform ablation experiments, modifying N_t , N_σ , and M individually with all the remaining parameters fixed. The results of these experiments are presented for $d = 1$ and $d = 2$, respectively, in Figures 6.1 and 6.2. We take $N = 10^4$ throughout; reference values for the other fixed parameters can be found in the captions.

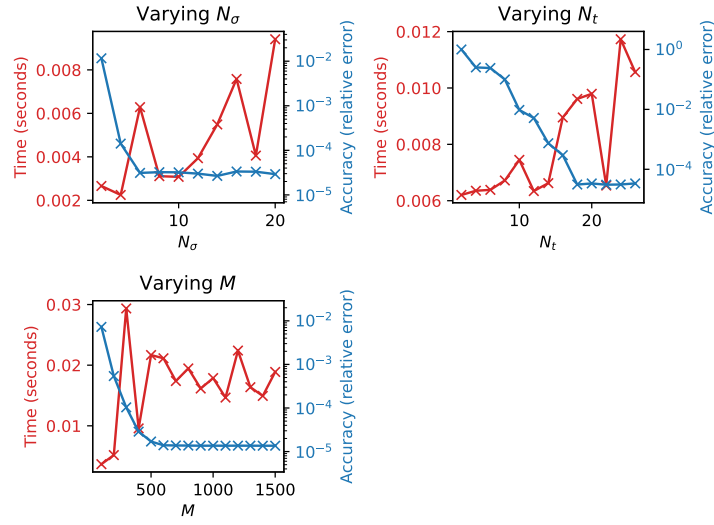


Figure 6.1: Matvec time and accuracy in one dimension for the Matérn kernel with $\nu = \frac{3}{2}$. Unless otherwise specified, $N_t = 20$, $N_\sigma = 20$, and $M = 400$. Results are averaged over 50 runs.

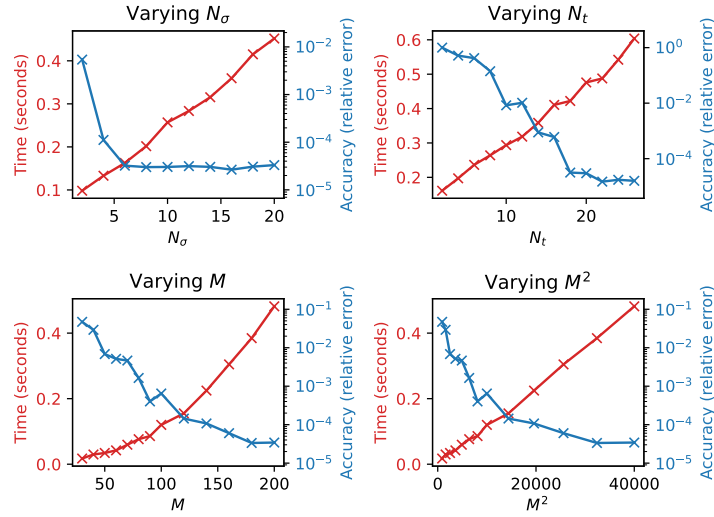


Figure 6.2: Matvec time and accuracy in two dimensions for the Matérn kernel with $\nu = \frac{3}{2}$. Unless otherwise specified, $N_t = 20$, $N_\sigma = 20$, and $M = 200$ ($M^2 = 40000$). Results are averaged over 3 runs.

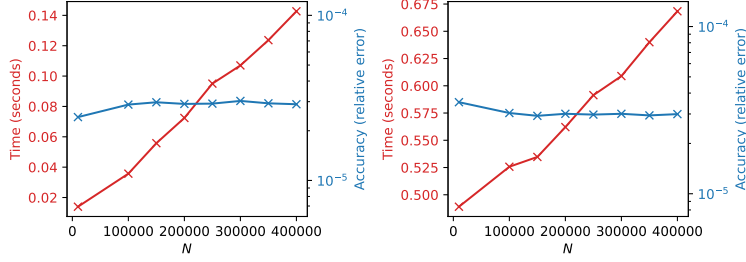


Figure 6.3: Matvec time and accuracy with varying N in $d = 1$ (left) and $d = 2$ (right) for the Matérn kernel with $\nu = \frac{3}{2}$. The reference values for N_t , N_σ , and M are the same as in Figures 6.1 and 6.2, respectively, as are the numbers of trial runs.

As expected, the time taken generally grows linearly in N_t , N_σ , and M^d , while errors decrease exponentially with N_t , N_σ , and M . In the one-dimensional case, our accuracy saturates with respect to M before the large- M asymptotic cost scaling is revealed, so the performance appears as roughly constant in M in these experiments. As we increase one parameter individually, the error will eventually saturate. This is consistent with our understanding in Theorem 14, in which each of these parameters contributes roughly independently to the error in an additive fashion. In the one-dimensional case especially, there is some variance in the time taken; this is because the matvec is sufficiently fast that smaller effects such as constant setup times fail to fully amortize.

Finally, maintaining the parameters at their given reference values for each case $d = 1, 2$, we vary N . The results are presented in Figure 6.3, showing approximately linear scaling independent of dimension and a constant relative error. The reference values for N_t , N_σ , and M are the same as in Figures 6.1 and 6.2.

We comment that in higher dimensions, the $O(M^d N_t N_\sigma)$ memory bottleneck of our most basic implementation becomes nontrivial. This bottleneck owes to the formation of the tensor $\hat{G}_{k,t_j}[\mathbf{n}, \mathbf{n}]$ (cf. Remark 1). A sequential implementation, in which the sums over k and j are processed sequentially, could reduce the memory bottleneck to $O(M^d)$, but we do not pursue such modifications.

Since the relative error is empirically independent of N , compatible with Theorem 14, we recommend an iterative approach to choosing parameters given a required error: repeatedly run test matvecs and increase one parameter, switching to another upon stagnation. This procedure can be employed for small N and then the choices can be extrapolated to larger regression problems.

Next we consider the same experiments in the case of the squared-exponential kernel, for which it is unnecessary to choose t_{\min} and t_{\max} , and there is no need to vary N_t . In this setting, $\rho_{\min} = \sigma_{\min}$, $\rho_{\max} = \sigma_{\max}$, and $\Delta\omega$ is determined accordingly. The results of the same ablation experiments for N_σ and M are presented in Figures 6.4, 6.5, and 6.6 for dimensions $d = 1, 2$, and 3, respectively. Once again, we take $N = 10^4$ throughout.

The time scaling in Figure 6.4 is not obvious because the error already saturates when M and N_σ are both very small. Increasing the parameters to a size where the scaling is more readily apparent would not be useful.

Once again, as expected, the error decays exponentially in N_σ and M , and the time grows linearly in N_σ and M^d . Since the integration in t no longer contributes to the error and since ρ_{\min} is larger

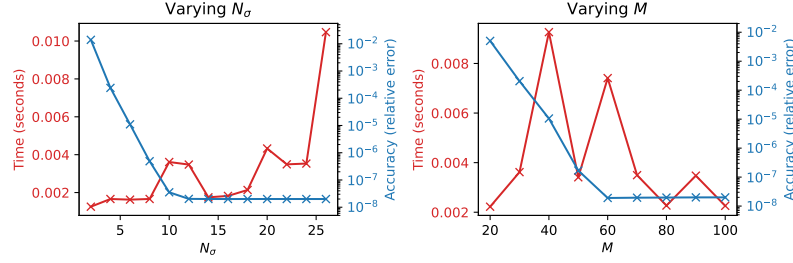


Figure 6.4: Matvec time and accuracy in one dimension for the squared-exponential kernel. Unless otherwise specified, $N_\sigma = 26$ and $M = 100$. Results are averaged over 5 runs.

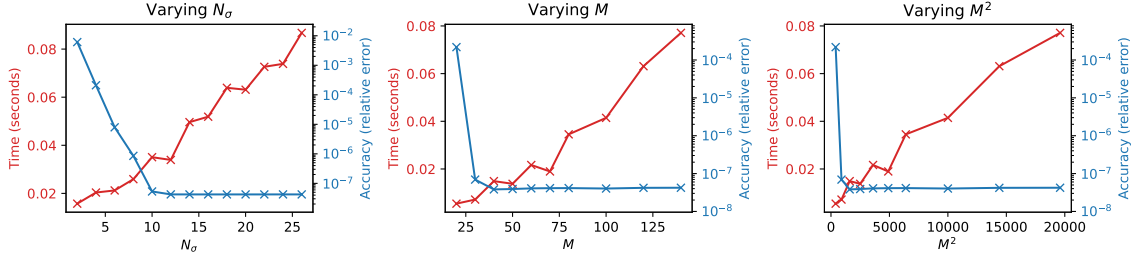


Figure 6.5: Matvec time and accuracy in two dimensions for the squared-exponential kernel. Unless otherwise specified, $N_\sigma = 26$ and $M = 140$. Results are averaged over 3 runs.

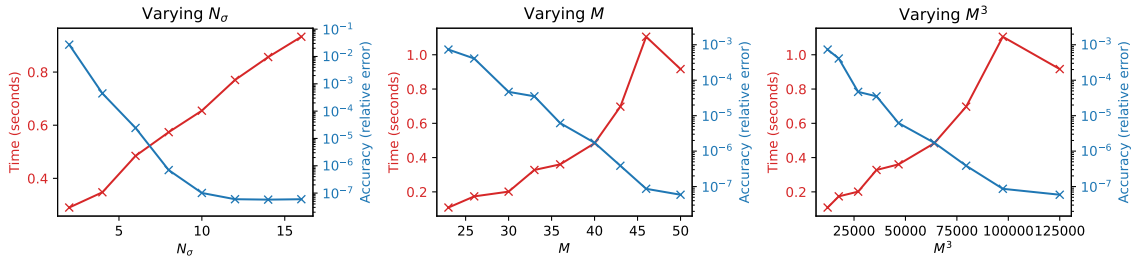


Figure 6.6: Matvec time and accuracy in three dimensions for the squared-exponential kernel. Unless otherwise specified, $N_\sigma = 16$ and $M = 50$. Results are shown for a single run.

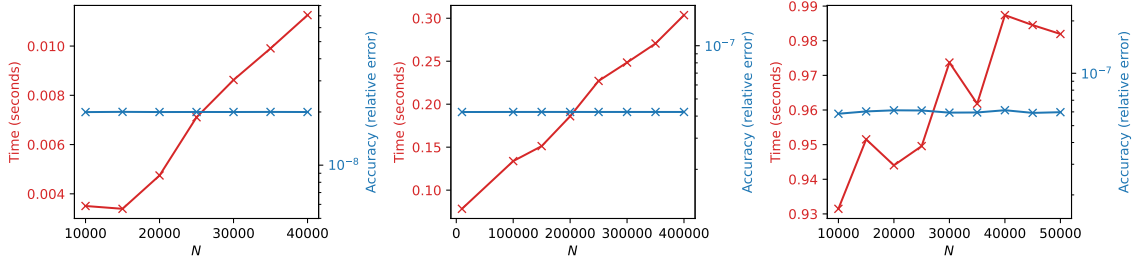


Figure 6.7: Matvec time and accuracy with varying N for the squared-exponential kernel, $d = 1, 2, 3$. The reference values for N_σ and M are the same as in Figures 6.4, 6.5, and 6.6, as are the numbers of trial runs.

(due to the fact that simply $\chi_{\min} = 1$), in this setting the error is smaller and the convergence with respect to M is faster, and we quickly hit the lower bound determined by the tolerance ϵ .

Finally, again keeping all parameters at their given reference values (defined in Figures 6.4, 6.5, and 6.6) and varying N , Figure 6.7 shows approximately linear scaling and constant relative error as in the Matérn case. For these experiments, we maintain relative accuracy of roughly 10^{-7} independent of N .

6.2 Solves

For the purposes of GPR, we are specifically interested in wrapping our kernel matvec subroutine in CG to compute the linear solve $(\mathbf{K} + \eta^2 I_N)\alpha = y$, cf. (1.1). Since the solve cost is fairly insensitive to the specification of y , we simply draw the entries of $y \in \mathbb{R}^N$ independently from the uniform distribution on $[0, 1]$.

We compare our results for this inversion to those of the MATLAB package FLAM [23], which was the fastest out of all alternative strategies tested in [20]. In this section, we focus on the squared-exponential kernel. We set $d = 2$, since for $d = 1$ the scaling of FLAM is linear in N and we believe that it remains a state-of-the-art approach.

FLAM and our method take different approaches. FLAM first computes a block factorization of the entire matrix $\mathbf{K} + \eta^2 I_N$ using elementwise queries. This is expensive but allows for fast matvecs and solves downstream. The Fourier method has insignificant offline cost but more expensive matvecs, and the solves require an iterative method wrapping the matvec subroutine. In order to compare the two, we consider the sum of both the on- and offline costs, i.e., the time necessary to go from no representation of \mathbf{K} at all to a complete solve of $(\mathbf{K} + \eta^2 I_N)\alpha = y$.

We consider two regimes, in both of which the condition number of the kernel matrix should remain approximately constant as N grows. Since our method uses an iterative solver, an increase in the condition number will increase its computational cost, while FLAM will remain relatively unaffected. Our method will be faster in the limit as $N \rightarrow \infty$ for any fixed condition number, but a change in conditioning could affect the crossover point. In the ill-conditioned case, we could also use a less-accurate and therefore cheaper FLAM factorization to provide a preconditioner in our approach, though we do not pursue this technique here.

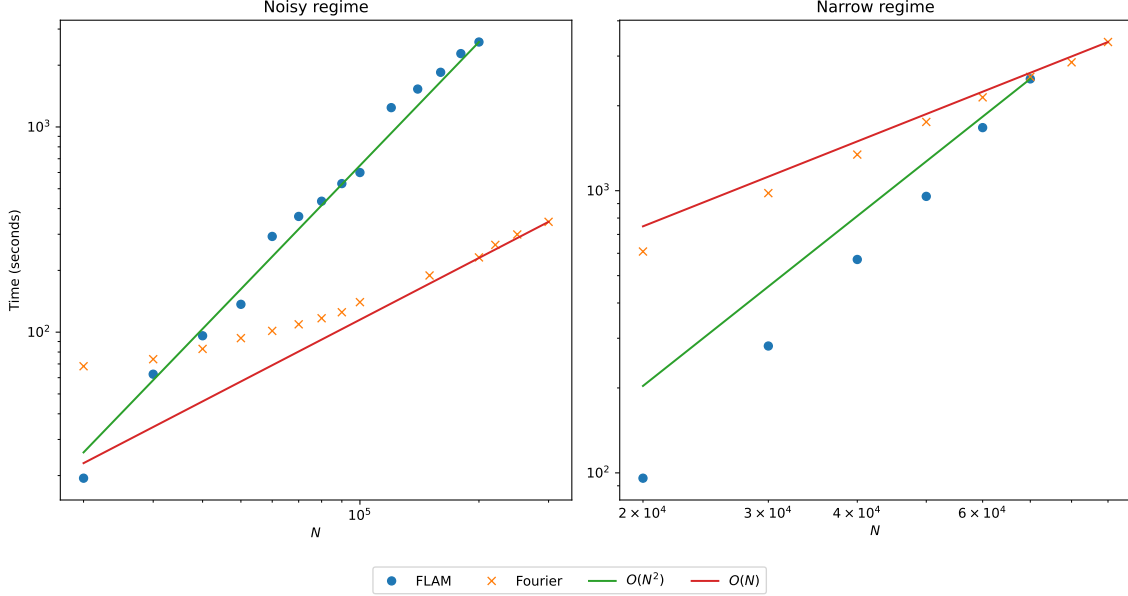


Figure 6.8: Time to perform the linear solve $(\mathbf{K} + \eta^2 I_N)\alpha = y$ for the squared exponential kernel in $d = 2$ in the scaling regimes discussed in Section 6.2.

In the first regime (the “noisy regime”), we take $\eta^2 = \Omega(N)$, specifically, $\eta^2 = \frac{N}{2 \times 10^6}$, while maintaining a constant kernel. In this scaling regime (the “noisy regime”), although we take an increasing number of observations, the noise of the observations also grows, such that our uncertainty about the inferred function remains constant. We fix $N_\sigma = 15$, $M = 75$, and $\epsilon = 10^{-6}$, and we choose a residual tolerance of 10^{-6} in CG. These choices yield relative matvec errors that are never larger than 10^{-5} .

In the second scaling regime (the “narrow regime”), we keep $\eta^2 = 10^{-1}$ constant, but change the kernel as N increases so that the effective number of nonzero entries in each row of \mathbf{K} remains constant and the diagonal entries of \mathbf{K} remain $\Omega(1)$. Specifically, in terms of our reference choice $\sigma_{\text{ref}}(x)$ for $\sigma(x)$, we set $\sigma(x) = (N/1000)^{-1/d} \sigma_{\text{ref}}(x)$ and $w(x) = (N/1000)^{-1/2}$ to fix the kernel. We set $N_\sigma = 15$, independent of N , and $M = 3N^{1/d}$ in order to maintain constant relative accuracy as N is increased. These choices yield relative matvec errors that are never larger than 10^{-5} . Again we choose a residual tolerance of 10^{-6} in CG. FLAM uses a recursive skeletonization algorithm, based on multiple interpolative decompositions (IDs) of submatrices. We set the tolerance for each ID to 10^{-10} and choose a tree occupancy parameter, which governs the size of the smallest submatrices to be factorized, of 200. The exact choice here is not particularly important in our experiments as long as it is substantially less than the size of the matrix. Both of these choices follow [20].

We report the cost comparison of the two approaches in Figure 6.8, and we show the relative residuals $\|(\mathbf{K} + \eta^2 I_N)\alpha - y\|/\|y\|$ obtained by each method in Figure 6.9, computed using the exact¹

¹The exact applications of \mathbf{K} required to compute the residuals were carried out in $O(N^2)$ time using the KeOps library [12]. Computing the solves this way would have been prohibitively slow, but a single application required only a few minutes for the largest values of N that we considered.

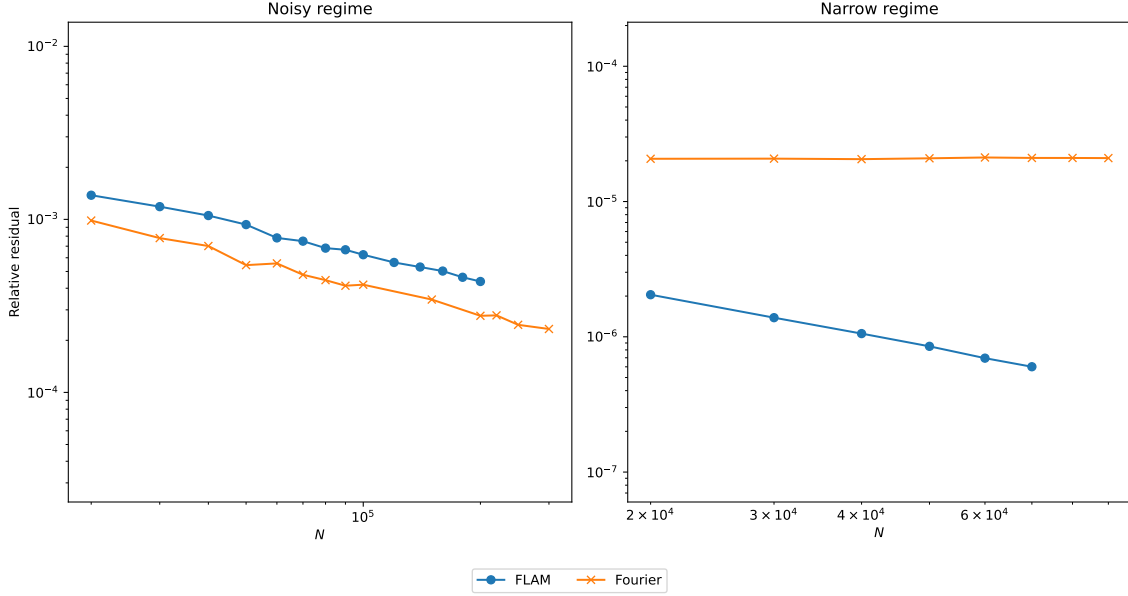


Figure 6.9: Relative residuals from performing the solve $(\mathbf{K} + \eta^2 I_N)\alpha = y$ for the squared exponential kernel in $d = 2$ in the scaling regimes discussed in Section 6.2.

kernel matrix \mathbf{K} . These figures confirm the $\tilde{O}(N)$ scaling of our method, which provides comparable residuals to those of FLAM, while the scaling of FLAM is at least $O(N^2)$ in both cases. (We use a naive implementation, in which we simply provide the FLAM library with a function for element- or block-wise access to the kernel matrix; more GPR-specific implementations using annular proxies can achieve $O(N^{3/2})$ scaling, which is still worse than the demonstrated scaling of our method [20].) The narrow regime uses smaller values of N compared to the noisy regime; this is due to both our implementation and FLAM running out of memory on the consumer hardware we used. For our method, this is caused by the scaling of $M^d = O(N)$ Fourier grid points in this regime, exacerbating the $O(M^d N_\sigma)$ memory bottleneck pointed out earlier in Section 6.1. The same memory restrictions kept us from experimenting with larger values of M and N_σ , which we would expect to bring the residuals in the narrow regime in line with those of FLAM. This memory bottleneck is straightforward to alleviate with a slightly modified implementation, as we have already commented in Section 6.1, in which we calculate the individual pointwise multiplications in Fourier space sequentially or in smaller batches. We defer any such alternative implementations, as well as analysis of the tradeoff between speed and memory, for future application-oriented work.

References

- [1] Sivaram Ambikasaran, Daniel Foreman-Mackey, Leslie Greengard, David W. Hogg, and Michael O’Neil. Fast Direct Methods for Gaussian Processes. *IEEE Transactions on Pattern Analysis and Machine Intelligence*, 38(2):252–265, February 2016.

- [2] Alex Barnett, Philip Greengard, and Manas Rachh. Uniform approximation of common Gaussian process kernels using equispaced Fourier grids. *Applied and Computational Harmonic Analysis*, 71:101640, July 2024.
- [3] Alex H. Barnett. Aliasing error of the $\exp(\beta\sqrt{1-z^2})$ kernel in the nonuniform fast Fourier transform. *Applied and Computational Harmonic Analysis*, 51:1–16, March 2021.
- [4] Alexander H. Barnett, Jeremy Magland, and Ludvig Af Klinteberg. A Parallel Nonuniform Fast Fourier Transform Library Based on an “Exponential of Semicircle” Kernel. *SIAM Journal on Scientific Computing*, 41(5):C479–C504, January 2019.
- [5] Albert P. Bartók, Mike C. Payne, Risi Kondor, and Gábor Csányi. Gaussian Approximation Potentials: The Accuracy of Quantum Mechanics, without the Electrons. *Physical Review Letters*, 104(13):136403, April 2010.
- [6] David Benisty. Quantifying the s_8 tension with the redshift space distortion data set. *Physics of the Dark Universe*, 31:100766, January 2021.
- [7] Gregory Beylkin and Lucas Monzón. On approximation of functions by exponential sums. *Applied and Computational Harmonic Analysis*, 19(1):17–48, July 2005.
- [8] Gregory Beylkin and Lucas Monzón. Approximation by exponential sums revisited. *Applied and Computational Harmonic Analysis*, 28(2):131–149, March 2010.
- [9] John P Boyd. A fast algorithm for chebyshev, fourier, and sinc interpolation onto an irregular grid. *Journal of Computational Physics*, 103(2):243–257, 1992.
- [10] John P. Boyd. *Chebyshev and Fourier spectral methods*. Dover Publications, Mineola, N.Y, 2nd ed., rev edition, 2001.
- [11] Seok-Ho Chang, Pamela C. Cosman, and Laurence B. Milstein. Chernoff-Type Bounds for the Gaussian Error Function. *IEEE Transactions on Communications*, 59(11):2939–2944, November 2011.
- [12] Benjamin Charlier, Jean Feydy, Joan Alexis Glaunès, François-David Collin, and Ghislain Durif. Kernel operations on the gpu, with autodiff, without memory overflows. *Journal of Machine Learning Research*, 22(74):1–6, 2021.
- [13] Noel Cressie. Mission CO₂ntrol: A Statistical Scientist’s Role in Remote Sensing of Atmospheric Carbon Dioxide. *Journal of the American Statistical Association*, 113(521):152–168, January 2018.
- [14] A. Dutt and V. Rokhlin. Fast fourier transforms for nonequispaced data. *SIAM Journal on Scientific Computing*, 14(6):1368–1393, 1993.
- [15] Daniel Foreman-Mackey, Eric Agol, Sivaram Ambikasaran, and Ruth Angus. Fast and Scalable Gaussian Process Modeling with Applications to Astronomical Time Series. *The Astronomical Journal*, 154(6):220, December 2017.
- [16] Reinhard Furrer, Marc G Genton, and Douglas Nychka. Covariance Tapering for Interpolation of Large Spatial Datasets. *Journal of Computational and Graphical Statistics*, 15(3):502–523, September 2006.

- [17] Andrew Gelman, John B. Carlin, Hal Steven Stern, David B. Dunson, Aki Vehtari, and Donald B. Rubin. *Bayesian data analysis*. Chapman & Hall/CRC texts in statistical science. CRC Press, Boca Raton, third edition. edition, 2014. OCLC: 909477393.
- [18] Leslie Greengard and John Strain. The fast gauss transform. *SIAM Journal on Scientific and Statistical Computing*, 12(1):79–94, January 1991.
- [19] Leslie F. Greengard, Shidong Jiang, Manas Rachh, and Jun Wang. A new version of the adaptive fast gauss transform for discrete and continuous sources. *SIAM Review*, 66(2):287–315, May 2024.
- [20] Philip Greengard, Manas Rachh, and Alex Barnett. Equispaced Fourier representations for efficient Gaussian process regression from a billion data points, May 2023. arXiv:2210.10210 [cs, math, stat].
- [21] Ryan-Rhys Griffiths, Jiachen Jiang, Douglas J. K. Buisson, Dan Wilkins, Luigi C. Gallo, Adam Ingram, Alpha A. Lee, Dirk Grupe, Erin Kara, Michael L. Parker, William Alston, Anthony Bourached, George Cann, Andrew Young, and S. Komossa. Modeling the multiwavelength variability of mrk 335 using gaussian processes. *The Astrophysical Journal*, 914(2):144, June 2021.
- [22] Matthew J. Heaton, Abhirup Datta, Andrew O. Finley, Reinhard Furrer, Joseph Guinness, Rajarshi Guhaniyogi, Florian Gerber, Robert B. Gramacy, Dorit Hammerling, Matthias Katzfuss, Finn Lindgren, Douglas W. Nychka, Furong Sun, and Andrew Zammit-Mangion. A Case Study Competition Among Methods for Analyzing Large Spatial Data. *Journal of Agricultural, Biological and Environmental Statistics*, 24(3):398–425, September 2019.
- [23] Kenneth Ho. FLAM: Fast Linear Algebra in MATLAB - Algorithms for Hierarchical Matrices. *Journal of Open Source Software*, 5(51):1906, July 2020.
- [24] Michael Kielstra and Michael Lindsey. Code for Gaussian process regression for common non-stationary kernels with log-linear scaling. <https://doi.org/10.5281/zenodo.12638456>, May 2025.
- [25] Per-Gunnar Martinsson. *Fast Direct Solvers for Elliptic PDEs*. Society for Industrial and Applied Mathematics, Philadelphia, PA, January 2019.
- [26] Victor Minden, Anil Damle, Kenneth L. Ho, and Lexing Ying. Fast Spatial Gaussian Process Maximum Likelihood Estimation via Skeletonization Factorizations. *Multiscale Modeling & Simulation*, 15(4):1584–1611, January 2017.
- [27] P. C. Mukesh Kumar and R. Kavitha. Prediction of nanofluid viscosity using multilayer perceptron and gaussian process regression. *Journal of Thermal Analysis and Calorimetry*, 144(4):1151–1160, May 2021.
- [28] Marcus M. Noack, Harinarayan Krishnan, Mark D. Risser, and Kristofer G. Reyes. Exact Gaussian processes for massive datasets via non-stationary sparsity-discovering kernels. *Scientific Reports*, 13(1):3155, 2023.
- [29] Marcus M. Noack, Hengrui Luo, and Mark D. Risser. A unifying perspective on non-stationary kernels for deeper Gaussian processes. *APL Machine Learning*, 2(1):010902, 02 2024.

- [30] Marcus M. Noack and James A. Sethian. Advanced stationary and nonstationary kernel designs for domain-aware Gaussian processes. *Communications in Applied Mathematics and Computational Science*, 17(1):131–156, October 2022.
- [31] E. J. Nyström. Über Die Praktische Auflösung von Integralgleichungen mit Anwendungen auf Randwertaufgaben. *Acta Mathematica*, 54(0):185–204, 1930.
- [32] C Paciorek. *Nonstationary Gaussian Processes for Regression and Spatial Modelling*. PhD thesis, Carnegie Mellon University, Pittsburgh, PA, 2003.
- [33] Christopher J. Paciorek and Mark J. Schervish. Spatial modelling using a new class of nonstationary covariance functions. *Environmetrics*, 17(5):483–506, August 2006.
- [34] Paciorek C and Schervish M. Nonstationary covariance functions for Gaussian process regression. In Thrun S, Saul L, and Schölkopf B, editors, *Advances in Neural Information Processing Systems 16*, pages 273–280. MIT Press, Cambridge, MA, 2004.
- [35] Inna Pustokhina, Amir Seraj, Hafsana Hafsana, Seyed Mojtaba Mostafavi, and S. M. Alizadeh. Developing a robust model based on the gaussian process regression approach to predict biodiesel properties. *International Journal of Chemical Engineering*, 2021:1–12, June 2021.
- [36] Carl Edward Rasmussen and Christopher K. I. Williams. *Gaussian processes for machine learning*. Adaptive computation and machine learning. MIT Press, Cambridge, Mass, 2006. OCLC: ocm61285753.
- [37] I. J. Schoenberg. Metric Spaces and Completely Monotone Functions. *Annals of Mathematics*, 39(4):811–841, 1938.
- [38] I. J. Schoenberg. Metric spaces and positive definite functions. *Transactions of the American Mathematical Society*, 44(3):522–536, 1938.
- [39] Y. Shih, G. Wright, J. Anden, J. Blaschke, and A. H. Barnett. cuFINUFFT: a load-balanced GPU library for general-purpose nonuniform FFTs. In *2021 IEEE International Parallel and Distributed Processing Symposium Workshops (IPDPSW)*, pages 688–697, Los Alamitos, CA, USA, jun 2021. IEEE Computer Society.
- [40] Marina Spivak, Shravan K. Veerapaneni, and Leslie Greengard. The fast generalized gauss transform. *SIAM Journal on Scientific Computing*, 32(5):3092–3107, January 2010.
- [41] Michael L. Stein. *Interpolation of Spatial Data*. Springer Series in Statistics. Springer New York, New York, NY, 1999.
- [42] Lloyd N. Trefethen. *Approximation theory and approximation practice*. SIAM, Society for Industrial and Applied Mathematics, Philadelphia, extended edition edition, 2020.
- [43] Lloyd N. Trefethen and David Bau. *Numerical linear algebra*. Society for Industrial and Applied Mathematics, Philadelphia, 1997.
- [44] Lloyd N. Trefethen and J. A. C. Weideman. The Exponentially Convergent Trapezoidal Rule. *SIAM Review*, 56(3):385–458, 2014.

- [45] Ke Alexander Wang, Geoff Pleiss, Jacob R. Gardner, Stephen Tyree, Kilian Q. Weinberger, and Andrew Gordon Wilson. *Exact gaussian processes on a million data points*, pages 14648–14659. Curran Associates Inc., Red Hook, NY, USA, 2019.

Appendices

A Glossary of notation

The following is a glossary of commonly used notation in our analysis. We think of d , ν , σ_{\min} , and σ_{\max} as given. We think of t_{\min} , t_{\max} , N_t , as well as N_σ and M , $\Delta\omega$ as tunable parameters controlling the error of the approximation. The other quantities are all induced in terms of these.

Terms	Meaning
d	Spatial dimension
ν	Matérn parameter (2.4)
t_{\min}, t_{\max}, N_t	Parameters for discretization scheme (3.10) of integral representation (cf. (3.3) and (3.8)) of the Matérn kernel
$\sigma_{\min}, \sigma_{\max}, N_\sigma, \kappa$	Parameters for Chebyshev interpolation by value of $\sigma(x) \in [\sigma_{\min}, \sigma_{\max}]$, cf. (3.13); $\kappa = \sigma_{\max}/\sigma_{\min}$.
Λ_{N_σ}	Lebesgue constant for the Chebyshev interpolation scheme, cf. Definition 9
χ_{\min}, χ_{\max}	$\chi_{\min} = \chi(t_{\min})$ and $\chi_{\max} = \chi(t_{\max})$, where $\chi(t)$ is defined in (3.8)
$\rho_{\min}, \rho_{\max}, \lambda$	$\rho_{\min} = \sigma_{\min}\chi_{\min}$, $\rho_{\max} = \sigma_{\max}\chi_{\max}$, and $\lambda = \rho_{\max}/\rho_{\min}$
$M, \Delta\omega$	Parameters defining Fourier grid $\Delta\omega \times \{-M, \dots, M\}^d$, cf. Section 3.4

B Integral representation of the kernel

Here we verify (3.4). Recalling the definition of \mathcal{B}_t , we compute:

$$\begin{aligned}
 (\mathcal{B}_t \mathcal{B}_t^*)(x, y) &= \int \mathcal{B}_t(x, z) \mathcal{B}_t(y, z) dz \\
 &= w(x) w(y) [2\pi \sigma(x) \sigma(y)]^{-d} \int e^{-\frac{|x-z|^2}{2\sigma^2(x)\chi^2(t)}} e^{-\frac{|y-z|^2}{2\sigma^2(y)\chi^2(t)}} dz.
 \end{aligned}$$

We can substitute the exact integration

$$\int e^{-\frac{|x-z|^2}{2\sigma(x)^2\chi(t)^2}} e^{-\frac{|y-z|^2}{2\sigma(y)^2\chi(t)^2}} dz = \left(\frac{2\pi\sigma^2(x)\sigma^2(y)\chi^2(t)}{\sigma^2(x) + \sigma^2(y)} \right)^{d/2} e^{-\frac{|x-y|^2}{2(\sigma^2(x) + \sigma^2(y))\chi^2(t)}}$$

to obtain

$$(\mathcal{B}_t \mathcal{B}_t^*)(x, y) v(t) = w(x) w(y) (2\pi [\sigma^2(x) + \sigma^2(y)])^{-d/2} e^{-\frac{|x-y|^2}{2(\sigma^2(x) + \sigma^2(y))\chi^2(t)}} u(t) \quad (\text{B.1})$$

Then using (3.3) to integrate against $u(t) dt$, we obtain

$$\int (\mathcal{B}_t \mathcal{B}_t^*)(x, y) v(t) dt = w(x) w(y) (2\pi [\sigma^2(x) + \sigma^2(y)])^{-d/2} \int e^{-\frac{|x-y|^2}{2(\sigma^2(x) + \sigma^2(y))\chi^2(t)}} u(t) dt$$

$$\begin{aligned}
&= w(x) w(y) (2\pi [\sigma^2(x) + \sigma^2(y)])^{-d/2} \varphi \left(\frac{|x - y|}{\sqrt{\sigma^2(x) + \sigma^2(y)}} \right) \\
&= \mathcal{K}(x, y).
\end{aligned}$$

This establishes the desired identity (3.4).

C Schoenberg representation of the Matérn function

We want to show how to present such $\varphi = \varphi_\nu$ in the form of (3.3) for suitably chosen $u(t)$ and $\chi(t)$.

It is useful to recall [41] that the Matérn function (2.4) can be more conveniently characterized in terms of a Fourier transform. Specifically, one can compute that

$$\psi(r) := \frac{\sqrt{\pi}}{2^{\nu-1} \Gamma(\nu + \frac{1}{2})} |r|^\nu K_\nu(r) = \int \frac{1}{(1 + \omega^2)^\beta} e^{i\omega r} d\omega, \quad (\text{C.1})$$

where $\beta = \nu + \frac{1}{2}$. In terms of ψ , we can write the Matérn function (2.4) $\varphi = \varphi_\nu$ as

$$\varphi(r) = \frac{\Gamma(\nu + \frac{1}{2})}{\sqrt{\pi} \Gamma(\nu)} \psi(\sqrt{2\nu} r). \quad (\text{C.2})$$

Now recall the identity [7]:

$$\frac{1}{(1 + \omega^2)^\beta} = \frac{1}{\Gamma(\beta)} \int e^{-e^t(1 + \omega^2) + \beta t} dt.$$

Then substitute into (C.1) to compute:

$$\begin{aligned}
\psi(r) &= \int \frac{1}{(1 + \omega^2)^\beta} e^{i\omega r} d\omega \\
&= \frac{1}{\Gamma(\beta)} \int \int e^{-e^t(1 + \omega^2) + \beta t} e^{i\omega r} d\omega dt \\
&= \frac{1}{\Gamma(\beta)} \int e^{\beta t - e^t} \left[\int e^{-e^t \omega^2} e^{i\omega r} d\omega \right] dt \\
&\stackrel{(\star)}{=} \frac{1}{\Gamma(\beta)} \int e^{\beta t - e^t} \sqrt{\frac{\pi}{e^t}} e^{-\frac{r^2}{4e^t}} dt \\
&= \frac{\sqrt{\pi}}{\Gamma(\beta)} \int e^{(\beta - \frac{1}{2})t - e^t} e^{-\frac{r^2}{4e^t}} dt.
\end{aligned} \quad (\text{C.3})$$

In the step indicated by (\star) we have used the identity for the inverse Fourier transform of a Gaussian.

Then plugging (C.3) into (C.2) and recalling that $\beta = \nu + \frac{1}{2}$, we obtain

$$\varphi(r) = \frac{1}{\Gamma(\nu)} \int e^{\nu t - e^t} e^{-\frac{r^2}{2e^t/\nu}} dt,$$

from which it directly follows that (3.3) holds with

$$u(t) := \frac{1}{\Gamma(\nu)} e^{\nu t - e^t}, \quad \chi(t) := \frac{1}{\sqrt{\nu}} e^{t/2}.$$

D Background on NUFFTs

In our algorithms we will make use of *non-uniform fast Fourier transforms (NUFFTs)* [9, 14] of both type 1 and type 2, which are in fact formal adjoints of one another.

For our purposes, the **type 1 NUFFT** takes as input a vector of values $(\alpha_j)_{j=1}^N$ associated to a scattered set of points $x_1, \dots, x_N \in \mathbb{R}^d$ and returns the object $\hat{\alpha}[\mathbf{n}]$ defined on elements $\mathbf{n} \in \mathbf{G} := \{-M, \dots, M\}^d$ of a truncated integer lattice by the formula $\hat{\alpha}[\mathbf{n}] = \sum_{j=1}^N \alpha_j e^{-2\pi i \mathbf{n} \cdot x_j}$. By rescaling the scattered points $x_j \rightarrow (\Delta\omega) x_j$, we can define the rescaled type-1 NUFFT:

$$\hat{\alpha}[\mathbf{n}] = \sum_{j=1}^N \alpha_j e^{-2\pi i (\mathbf{n}\Delta\omega) \cdot x_j},$$

which can be viewed as the evaluation of the unitary Fourier transform \mathcal{F} of the empirical distribution $\sum_{j=1}^N \alpha_j \delta_{x_j}$ on the Fourier grid $\{\mathbf{n}\Delta\omega : \mathbf{n} \in \mathbf{G}\}$:

$$\hat{\alpha}[\mathbf{n}] = \left(\mathcal{F} \left[\sum_{j=1}^N \alpha_j \delta_{x_j} \right] \right) (\mathbf{n}\Delta\omega).$$

The **type 2 NUFFT** (including our rescaling convention), takes such a grid function f as input and returns a vector $\hat{f} = (\hat{f}_j)_{j=1}^N$ of values associated to the scattered points, defined by:

$$\hat{f}_j = \sum_{\mathbf{n} \in \mathbf{G}} f[\mathbf{n}] e^{2\pi i (\mathbf{n}\Delta\omega) \cdot x_j}.$$

Importantly, although the NUFFTs of type 1 and 2 are formal adjoints of one another, they are not inverses of one another.

Both types of NUFFT can be computed approximately (with prescribed accuracy) using standard libraries with $O(M^d + N \log N)$ computational cost [4]. All of our computations make use of the FiNUFFT library [4, 39, 3]. In this work, we assume for simplicity that we can compute NUFFTs exactly, neglecting this source of approximation error. We comment here that the scaling of the runtime of the NUFFT with respect to the prescribed error is merely logarithmic and can be easily accounted for. We elide this source of error simply for clarity of presentation.

E Proofs of technical lemmata

Proof of Lemma 3. Without loss of generality assume that $\|A\| = 1$. Then letting $x \in \mathbb{R}^N$ with $\|x\|_p = 1$, we want to show that $\|Ax\|_p \leq N$. Let a_i be the i -th row of A , and let q be such that $1/p + 1/q = 1$. Then $\|a_i\|_q \leq N^{1/q}$ follows from $\|A\| = 1$ for all $i = 1, \dots, N$. Finally, we can use Hölder's inequality to bound

$$\|Ax\|_p^p = \sum_{i=1}^N |a_i \cdot x|^p \leq \sum_{i=1}^N \|a_i\|_q^p \|x\|_p^p \leq N^{p/q+1} = N^p,$$

which completes the proof. \square

Proof of Lemma 4. Recalling our expression (3.7) for $(\mathcal{B}_t \mathcal{B}_t^*)(x, y) v(t)$, our assumption (5.1) bounding $|w(x)| \leq 1$, and our Matérn function representation (3.8), compute:

$$\begin{aligned} |(\mathcal{B}_t \mathcal{B}_t^*)(x, y) v(t)| &= \left| w(x) w(y) (2\pi [\sigma^2(x) + \sigma^2(y)])^{-d/2} e^{-\frac{|x-y|^2}{2(\sigma(x)^2 + \sigma(y)^2)\chi(t)^2}} u(t) \right| \\ &\leq (2\pi)^{-d/2} \sigma_{\min}^{-d} u(t) \\ &= O\left(\sigma_{\min}^{-d} e^{\nu t - e^t}\right). \end{aligned}$$

In summary, by Definition 2 of the norm $\|\cdot\|$,

$$\|\mathcal{B}_t \mathcal{B}_t^* v(t)\| = O\left(\sigma_{\min}^{-d} e^{\nu t - e^t}\right). \quad (\text{E.1})$$

Now, extending our definition $t_j = t_{\min} + j \Delta t$ to all integers $j \in \mathbb{Z}$ (where we recall that $\Delta t = (t_{\max} - t_{\min})/N_t$), we bound by the triangle inequality:

$$\begin{aligned} \left\| \mathcal{K} - \sum_{j=0}^{N_t} (\mathcal{B}_{t_j} \mathcal{B}_{t_j}^*) v_j \right\| &\leq \left\| \mathcal{K} - \sum_{j=-\infty}^{\infty} (\mathcal{B}_{t_j} \mathcal{B}_{t_j}^*) v(t_j) \Delta t \right\| \\ &\quad + \sum_{j=-\infty}^0 \left\| \mathcal{B}_{t_j} \mathcal{B}_{t_j}^* v(t_j) \right\| \Delta t + \sum_{j=N_t}^{\infty} \left\| \mathcal{B}_{t_j} \mathcal{B}_{t_j}^* v(t_j) \right\| \Delta t. \\ &= \left\| \mathcal{K} - \sum_{j=-\infty}^{\infty} (\mathcal{B}_{t_j} \mathcal{B}_{t_j}^*) v(t_j) \Delta t \right\| \\ &\quad + O\left(\sigma_{\min}^{-d} \sum_{j=-\infty}^0 e^{\nu t_j - e^{t_j}} \Delta t + \sigma_{\min}^{-d} \sum_{j=N_t}^{\infty} e^{\nu t_j - e^{t_j}} \Delta t\right), \end{aligned} \quad (\text{E.2})$$

where in the last step we have used (E.1). In the last expression, the first error term measures the error of the infinite Riemann sum approximation of $\mathcal{K} = \int_{-\infty}^{\infty} \mathcal{B}_t \mathcal{B}_t^* v(t) dt$, while the last term measures the effect of cutting off the tails of the Riemann sum.

The impact of the tails can be bounded as follows. First compute:

$$\sum_{j=-\infty}^0 e^{\nu t_j - e^{t_j}} \Delta t \leq \Delta t \sum_{j=-\infty}^0 e^{\nu t_j} = e^{\nu t_{\min}} (\Delta t) \sum_{j=0}^{\infty} e^{-(\nu \Delta t)j} = e^{\nu t_{\min}} \frac{\Delta t}{1 - e^{-\nu \Delta t}},$$

so it follows that

$$\sum_{j=-\infty}^0 e^{\nu t_j - e^{t_j}} \Delta t = O(e^{\nu t_{\min}}), \quad (\text{E.3})$$

as long as $\Delta t = O(1)$.

Next, note that by convexity, $e^t \geq e^{t_0} + (t - t_0)e^{t_0}$ for any t_0 . Choose $t_0 = \log(\nu + \alpha)$ for arbitrary $\alpha > 0$, yielding

$$e^t \geq (\nu + \alpha)t + (\nu + \alpha)(1 - \log(\nu + \alpha)).$$

Therefore

$$\sum_{j=N_t}^{\infty} e^{\nu t_j - e^{t_j}} \leq e^{-(\nu + \alpha)(1 - \log(\nu + \alpha))} \sum_{j=N_t}^{\infty} e^{-\alpha t_j} dt = e^{-(\nu + \alpha)(1 - \log(\nu + \alpha))} \frac{e^{-\alpha t_{\max}}}{1 - e^{-\nu \Delta t}},$$

and it follows that

$$\sum_{j=N_t}^{\infty} e^{\nu t_j - e^{t_j}} \Delta t \leq e^{-(\nu + \alpha)(1 - \log(\nu + \alpha))} e^{-\alpha t_{\max}} \frac{\Delta t}{1 - e^{-\nu \Delta t}} = O(e^{-\alpha t_{\max}}). \quad (\text{E.4})$$

Then combining (E.3) and (E.4) with (E.2), we have that for any $\alpha > 0$,

$$\left\| \mathcal{K} - \sum_{j=0}^{N_t} (\mathcal{B}_{t_j} \mathcal{B}_{t_j}^*) v_j \right\| \leq \left\| \mathcal{K} - \sum_{j=-\infty}^{\infty} (\mathcal{B}_{t_j} \mathcal{B}_{t_j}^*) v(t_j) \Delta t \right\| + O(\sigma_{\min}^{-d} [e^{-\alpha t_{\max}} + e^{\nu t_{\min}}]). \quad (\text{E.5})$$

It remains to bound the first term on the right-hand side of (E.5), i.e., the error of the infinite Riemann sum.

Specifically, we want to show that for any $\delta \in (0, 1)$,

$$\left\| \mathcal{K} - \sum_{j=-\infty}^{\infty} (\mathcal{B}_{t_j} \mathcal{B}_{t_j}^*) v(t_j) \Delta t \right\| = O\left(\sigma_{\min}^{-d} e^{-\frac{(1-\delta)\pi^2}{\Delta t}}\right), \quad (\text{E.6})$$

which, together with (E.5), will complete the proof.

For simplicity, fix x, y and define

$$f(t) := e^{-\frac{|x-y|^2}{2(\sigma(x)^2 + \sigma(y)^2)\chi(t)^2}} e^{\nu t - e^t}. \quad (\text{E.7})$$

Then, by our expression (3.7) for $(\mathcal{B}_t \mathcal{B}_t^*)(x, y) v(t)$, our assumption (5.1) bounding $|w(x)| \leq 1$, and our Matérn function representation (3.8), it suffices to show that the error of the infinite Riemann sum for $f(t)$ is $O\left(e^{-\frac{(1-\delta)\pi^2}{\Delta t}}\right)$, independent of x, y .

Standard results [44] guarantee that if we extend f analytically to a strip

$$T := \{z \in \mathbb{C} : |\text{Im}(z)| < B\}$$

where $B > 0$ and can find $M > 0$ bounding

$$\int_{-\infty}^{\infty} |f(a + ib)| da \leq M$$

uniformly over $b \in (-B, B)$, then the error of the Riemann sum is bounded by

$$\frac{2M}{e^{2\pi B/\Delta t} - 1}.$$

We will take $B = (1 - \delta)\frac{\pi}{2}$, so the proof is complete once we can show that

$$\int_{-\infty}^{\infty} |f(a + ib)| da = O(1), \quad (\text{E.8})$$

independent of x, y and $|b| \leq (1 - \delta)\frac{\pi}{2}$.

For $t = a + ib$ with $|b| \leq (1 - \delta)\frac{\pi}{2}$, let us bound the size of the first factor in the definition (E.7) of $f(t)$, using the fact that $\chi^2(t) = \nu^{-1}e^t$:

$$\left| e^{-\frac{|x-y|^2}{2\nu^{-1}(\sigma(x)^2 + \sigma(y)^2)e^t}} \right| = \left| e^{-e^{-t}} \right|^{\frac{|x-y|^2}{2\nu^{-1}(\sigma(x)^2 + \sigma(y)^2)}}. \quad (\text{E.9})$$

Now

$$\left| e^{-e^{-t}} \right| = e^{-\text{Re}[e^{-t}]} = e^{-e^{-a} \cos(b)},$$

and since $|b| < \pi/2$, we have $e^{-a} \cos(b) > 0$, and therefore $\left| e^{-e^{-t}} \right| \leq 1$. Moreover, the power $\frac{|x-y|^2}{2\nu^{-1}(\sigma(x)^2 + \sigma(y)^2)}$ is non-negative, so the entirety of (E.9) is bounded by 1 on T , i.e.,

$$\left| e^{-\frac{|x-y|^2}{2\nu^{-1}(\sigma(x)^2 + \sigma(y)^2)e^t}} \right| \leq 1 \quad (\text{E.10})$$

for $t = a + ib$ where $|b| \leq (1 - \delta)\frac{\pi}{2}$.

Next, let us bound the size of the second factor in the definition (E.7) of $f(t)$:

$$\left| e^{\nu t - e^t} \right| = e^{\text{Re}[\nu t - e^t]} = e^{\nu a - e^a \cos(b)}.$$

Now $|b| < B := (1 - \delta)\frac{\pi}{2}$, so $\cos(b) \geq \cos(B) > 0$, so

$$\left| e^{\nu t - e^t} \right| \leq e^{\nu a - \cos(B)e^a}. \quad (\text{E.11})$$

Therefore, combining (E.10) and (E.11) with the definition (E.7) of $f(t)$, we obtain

$$\int_{-\infty}^{\infty} |f(a + ib)| da \leq \int_{-\infty}^{\infty} e^{\nu a - \cos(B)e^a} da.$$

The right-hand side is integrable since $\cos(B) > 0$ and independent of x, y , as well as the choice of $b \in (-B, B)$, so we have achieved (E.8) and the proof is complete. \square

Proof of Lemma 6. Our proof will leverage the well-known error bound for Chebyshev interpolation given by Theorem 8.2 of [42]. To use this error bound, we make a few preliminary comments. First, recall that the *Bernstein ellipse* E_ρ of radius $\rho > 1$ is defined to be the subset

$$E_\rho = \left\{ \frac{\rho e^{i\theta} + \rho^{-1} e^{-i\theta}}{2} : \theta \in [0, 2\pi) \right\} = \left\{ z \in \mathbb{C} : \frac{\text{Re}(z)^2}{\left[\frac{\rho + \rho^{-1}}{2} \right]^2} + \frac{\text{Im}(z)^2}{\left[\frac{\rho - \rho^{-1}}{2} \right]^2} \right\}$$

of the complex plane.

Second, let $\sigma(s) := \sigma_{\min} + \frac{s+1}{2}(\sigma_{\max} - \sigma_{\min})$ be the affine transformation that maps the standard reference interval $[-1, 1]$ for Chebyshev interpolation to our interpolation interval $[\sigma_{\min}, \sigma_{\max}]$. We can view this map $\sigma(s)$ as extending to the entire complex plane.

Now Theorem 8.2 of [42] directly implies that if there exists some constant M such that $\left| e^{-\frac{x^2}{2\sigma(s)^2}} \right| \leq M$ for all $s \in E_\rho$ and all $x \in \mathbb{R}$, then

$$\left| e^{-\frac{x^2}{2\sigma(t)^2}} - \sum_{k=1}^{N_\sigma} P_k(\sigma(t)) e^{-\frac{x^2}{2\sigma_k^2}} \right| \leq \frac{4M}{\rho-1} \rho^{-N_\sigma} \quad (\text{E.12})$$

for all $\sigma(t) \in [\sigma_{\min}, \sigma_{\max}]$ and all $x \in \mathbb{R}$. Therefore, we want to find constants $\rho > 1$ and M such that the bound

$$\left| e^{-\frac{x^2}{2\sigma(s)^2}} \right| \leq M \quad (\text{E.13})$$

holds for all $s \in E_\rho$ and $x \in \mathbb{R}$.

To achieve this, we start by writing $s = a + bi$ for $a, b \in \mathbb{R}$. Then

$$\sigma_{\min}^{-1} \sigma(s) = [1 + \lambda + a\lambda] + [b\lambda]i,$$

where we have defined $\lambda := \frac{1}{2}(\kappa - 1) \geq 0$. Further define $\alpha := 1 + \lambda + a\lambda$ and $\beta := b\lambda$, so that

$$\sigma(s) = (\alpha + \beta i) \sigma_{\min}.$$

Then we can write

$$\begin{aligned} \left| e^{-\frac{x^2}{2\sigma(s)^2}} \right| &= \left| \exp \left[- \left(\frac{x}{\sqrt{2}\sigma_{\min}} \right)^2 (\alpha + \beta i)^{-2} \right] \right| \\ &= \exp \left[- \left(\frac{x}{\sqrt{2}\sigma_{\min}} \right)^2 \operatorname{Re} [(\alpha + \beta i)^{-2}] \right] \\ &= \exp \left[\left(\frac{x}{\sqrt{2}\sigma_{\min}} \right)^2 \frac{\beta^2 - \alpha^2}{(\alpha^2 + \beta^2)^2} \right]. \end{aligned}$$

It will follow that

$$\left| e^{-\frac{x^2}{2\sigma(s)^2}} \right| \leq 1$$

as long as we can guarantee that $\beta^2 \leq \alpha^2$.

Then we claim that under the choice

$$\rho = \frac{\lambda + 1}{\lambda}, \quad (\text{E.14})$$

the desired inequality (E.13) holds with $M = 1$. The preceding argument establishes that to prove this claim, it suffices to show that $\beta^2 \leq \alpha^2$ whenever $s \in E_\rho$.

To wit, we want to show that

$$(b\lambda)^2 \leq (1 + \lambda + a\lambda)^2$$

for all $a + ib \in E_\rho$. To see this, in turn it suffices to show that

$$|b|\lambda \leq 1 + \lambda + a\lambda.$$

Now recall that any $s = a + ib \in E_\rho$ satisfies $|a| \leq \frac{1}{2}(\rho + \rho^{-1})$ and $|b| \leq \frac{1}{2}(\rho - \rho^{-1})$. Thus in turn it suffices to show that

$$\frac{1}{2}(\rho - \rho^{-1})\lambda \leq 1 + \lambda - \frac{1}{2}(\rho + \rho^{-1})\lambda. \quad (\text{E.15})$$

Algebraic manipulations verify that the choice (E.14) ensures that (E.15) holds with equality.

Therefore (E.13) holds with $M = 1$ and $\rho = \frac{\lambda+1}{\lambda}$. Since in turn $\lambda = \frac{1}{2}(\kappa - 1)$, the statement of the lemma directly follows from substitution and simplification. \square

Proof of Lemma 10. We introduce an intermediate quantity $\mathcal{B}_t \mathcal{B}_t^{(N_\sigma)*}$ and then expand the definitions of \mathcal{B}_t (3.5) and $\mathcal{B}_t^{(N_\sigma)}$ (3.16), recalling our assumption (5.1) that $|w(x)| \leq 1$:

$$\begin{aligned} & \left| \left(\mathcal{B}_t \mathcal{B}_t^* - \mathcal{B}_t^{(N_\sigma)} \mathcal{B}_t^{(N_\sigma)*} \right) (x, y) \right| \\ & \leq \left| \left(\mathcal{B}_t \mathcal{B}_t^* - \mathcal{B}_t \mathcal{B}_t^{(N_\sigma)*} \right) (x, y) \right| + \left| \left(\mathcal{B}_t \mathcal{B}_t^{(N_\sigma)*} - \mathcal{B}_t^{(N_\sigma)} \mathcal{B}_t^{(N_\sigma)*} \right) (x, y) \right| \\ & \leq \left| \int_{\mathbb{R}^d} e^{-\frac{|x-z|^2}{2\sigma^2(x)\chi^2(t)}} e^{-\frac{|y-z|^2}{2\sigma^2(y)\chi^2(t)}} dz - \sum_{j=0}^{N_\sigma} P_j(\sigma(x)) \int_{\mathbb{R}^d} e^{-\frac{|x-z|^2}{2\sigma_j^2\chi(t)^2}} e^{-\frac{|y-z|^2}{2\sigma^2(y)\chi^2(t)}} dz \right| \\ & \quad + \left| \sum_{j=0}^{N_\sigma} P_j(\sigma(x)) \int_{\mathbb{R}^d} e^{-\frac{|x-z|^2}{2\sigma_j^2\chi(t)^2}} e^{-\frac{|y-z|^2}{2\sigma^2(y)\chi^2(t)}} dz - \sum_{j,k=0}^{N_\sigma} P_j(\sigma(x)) P_k(\sigma(y)) \int_{\mathbb{R}^d} e^{-\frac{|x-z|^2}{2\sigma_j^2\chi^2(t)}} e^{-\frac{|y-z|^2}{2\sigma_k^2\chi^2(t)}} dz \right| \\ & = \left| \int_{\mathbb{R}^d} e^{-\frac{|y-z|^2}{2\sigma^2(y)\chi^2(t)}} \left(e^{-\frac{|x-z|^2}{2\sigma^2(x)\chi^2(t)}} - \sum_{j=0}^{N_\sigma} P_j(\sigma(x)) e^{-\frac{|x-z|^2}{2\sigma_j^2\chi(t)^2}} \right) dz \right| \\ & \quad + \left| \sum_{j=0}^{N_\sigma} P_j(\sigma(x)) \int_{\mathbb{R}^d} e^{-\frac{|x-z|^2}{2\sigma_j^2\chi^2(t)}} \left(e^{-\frac{|y-z|^2}{2\sigma^2(y)\chi^2(t)}} - \sum_{k=0}^{N_\sigma} P_k(\sigma(y)) e^{-\frac{|y-z|^2}{2\sigma_k^2\chi^2(t)}} \right) dz \right| \\ & \leq \int_{\mathbb{R}^d} e^{-\frac{|y-z|^2}{2\sigma^2(y)\chi^2(t)}} \left| e^{-\frac{|x-z|^2}{2\sigma^2(x)\chi^2(t)}} - \sum_{j=0}^{N_\sigma} P_j(\sigma(x)) e^{-\frac{|x-z|^2}{2\sigma_j^2\chi(t)^2}} \right| dz \\ & \quad + \sum_{j=0}^{N_\sigma} |P_j(\sigma(x))| \int_{\mathbb{R}^d} e^{-\frac{|x-z|^2}{2\sigma_j^2\chi^2(t)}} \left| e^{-\frac{|y-z|^2}{2\sigma^2(y)\chi^2(t)}} - \sum_{k=0}^{N_\sigma} P_k(\sigma(y)) e^{-\frac{|y-z|^2}{2\sigma_k^2\chi^2(t)}} \right| dz \end{aligned}$$

Now we apply Lemma 6 twice to bound each of the differences between absolute value bars in the last expression, yielding:

$$\left| \left(\mathcal{B}_t \mathcal{B}_t^* - \mathcal{B}_t^{(N_\sigma)} \mathcal{B}_t^{(N_\sigma)*} \right) (x, y) \right| \leq \epsilon_{\text{cheb}} \int_{\mathbb{R}^d} e^{-\frac{|y-z|^2}{2\sigma^2(y)\chi^2(t)}} dz + \epsilon_{\text{cheb}} \sum_{j=0}^{N_\sigma} |P_j(\sigma(x))| \int_{\mathbb{R}^d} e^{-\frac{|x-z|^2}{2\sigma_j^2\chi^2(t)}} dz. \quad (\text{E.16})$$

Then for $\sigma \leq \sigma_{\max}$ and $\chi \leq \chi_{\max}$, we have

$$\int_{\mathbb{R}^d} e^{-\frac{|y-z|^2}{2\sigma^2\chi^2}} dz = O(\rho_{\max}^d).$$

Therefore from (E.16) and Definition 9 (of the Lebesgue constant), it follows that

$$\left| \left(\mathcal{B}_t \mathcal{B}_t^* - \mathcal{B}_t^{(N_\sigma)} \mathcal{B}_t^{(N_\sigma)*} \right) (x, y) \right| = O(\epsilon_{\text{cheb}}(1 + \Lambda_{N_\sigma})\rho_{\max}^d),$$

independently of x, y , from which the desired statement follows. \square

Proof of Lemma 11. For all $k = 0, \dots, N_\sigma$, define

$$g_{k,t,x}(z) = e^{-\frac{|x-z|^2}{2\sigma_k^2\chi^2(t)}},$$

so that $\mathcal{G}_{k,t}$ (defined as in (3.15)) satisfies

$$\mathcal{G}_{k,t}(x, z) = g_{k,t,x}(z).$$

Moreover, let $\hat{g}_{k,t,x} := \mathcal{F}g_{k,t,x}$ denote the Fourier transform of this function.

Define the index set $\mathbf{G} := \{-M, \dots, M\}^d$ for our Fourier grid, and let $\omega_{\mathbf{n}} := \mathbf{n}\Delta\omega$ denote the Fourier grid points themselves for $\mathbf{n} \in \mathbf{G}$.

Then observe that

$$\begin{aligned} (\Delta\omega)^d [\mathcal{G}_{k,t} \mathcal{F}^* \Pi^* \Pi \mathcal{F} \mathcal{G}_{l,t}] (x, y) &= (\Delta\omega)^d [(\Pi \mathcal{F} \mathcal{G}_{k,t})^* (\Pi \mathcal{F} \mathcal{G}_{l,t})] (x, y) \\ &= (\Delta\omega)^d \sum_{\mathbf{n} \in \mathbf{G}} \overline{\hat{g}_{k,t,x}(\omega_{\mathbf{n}})} \hat{g}_{l,t,y}(\omega_{\mathbf{n}}), \end{aligned}$$

and meanwhile

$$[\mathcal{G}_{k,t} \mathcal{G}_{l,t}] (x, y) = [\mathcal{G}_{k,t} \mathcal{F}^* \mathcal{F} \mathcal{G}_{l,t}] (x, y) = \int \overline{\hat{g}_{k,t,x}(\omega)} \hat{g}_{l,t,y}(\omega) d\omega.$$

Therefore to prove the lemma, we simply need to bound the error of the trapezoidal rule on our Fourier grid defined by $(M, \Delta\omega)$ for the integration of the function

$$\hat{f}_{k,l,x,y,t}(\omega) := \overline{\hat{g}_{k,t,x}(\omega)} \hat{g}_{l,t,y}(\omega),$$

independently of $t \in [t_{\min}, t_{\max}]$, $k, l \in \{0, \dots, N_\sigma\}$, and $x, y \in [-1, 1]^d$. We will write $\hat{f} = \hat{f}_{k,l,x,y,t}$ for notational simplicity. Concretely then we want to bound the integral error

$$I := \left| \int_{\mathbb{R}^d} \hat{f}(\omega) d\omega - (\Delta\omega)^d \sum_{\mathbf{n} \in \mathbf{G}} \hat{f}(\mathbf{n} \Delta\omega) \right|.$$

We can compute directly the Fourier transform of the Gaussian

$$\hat{g}_{k,t,x}(\omega) = \left(\sqrt{2\pi} \sigma_k \chi(t) \right)^d e^{-2\pi i \omega \cdot x} e^{-[2\pi \sigma_k \chi(t)]^2 \frac{|\omega|^2}{2}}$$

and hence also the analytical formula

$$\hat{f}(\omega) = (2\pi \sigma_k \sigma_l \chi^2(t))^d e^{2\pi i \omega \cdot (x-y)} e^{-\frac{[2\pi \sigma_k \chi(t)]^2 + [2\pi \sigma_l \chi(t)]^2}{2} |\omega|^2}. \quad (\text{E.17})$$

Then bound

$$I \leq \underbrace{\left| \int_{\mathbb{R}^d} \hat{f}(\omega) d\omega - (\Delta\omega)^d \sum_{\mathbf{n} \in \mathbb{Z}^d} \hat{f}(\mathbf{n} \Delta\omega) \right|}_{=: I_1} + \underbrace{(\Delta\omega)^d \sum_{\mathbf{n} \in \mathbb{Z}^d \setminus \mathbf{G}} |\hat{f}(\mathbf{n} \Delta\omega)|}_{=: I_2}. \quad (\text{E.18})$$

The first term on the right-hand side of (E.18) measures the error of the infinite Riemann sum approximation of $\int_{\mathbb{R}^d} \hat{f}(\omega) d\omega$. The second term measures the effect of cutting off the tails of \hat{f} .

To bound the second term, we deduce from (E.17) that

$$|\hat{f}(\omega)| = O\left(\rho_{\max}^{2d} e^{-[2\pi \rho_{\min} |\omega|]^2}\right), \quad (\text{E.19})$$

from which it follows² that the tail term can be bounded as

$$I_2 = O\left(\rho_{\max}^d \lambda^d e^{-[2\pi \rho_{\min} M \Delta\omega]^2}\right), \quad (\text{E.20})$$

²We can bound $I_2 \leq C \rho_{\max}^{2d} (\Delta\omega)^d \sum_{\mathbf{n} \in \mathbb{Z}^d \setminus \mathbf{G}} e^{-[2\pi \rho_{\min} \Delta\omega]^2 |\mathbf{n}|^2}$ using (E.19), for a suitable constant $C > 0$. Then we can bound the sum over $\mathbb{Z}^d \setminus \mathbf{G}$ with the sum of the sums over each of the ‘slab complements’ $\{\mathbf{n} : |n_i| > M\}$ for $i = 1, \dots, d$, which are all equal, yielding:

$$\begin{aligned} I_2 &\leq C d \rho_{\max}^{2d} (\Delta\omega)^d \sum_{|n_1| > M} \sum_{n_2, \dots, n_d = -\infty}^{\infty} e^{-[2\pi \rho_{\min} \Delta\omega]^2 |\mathbf{n}|^2} \\ &= C d \rho_{\max}^{2d} \left[\Delta\omega \sum_{n=-\infty}^{\infty} e^{-[2\pi \rho_{\min} \Delta\omega]^2 n^2} \right]^{d-1} \left[\Delta\omega \sum_{|n| > M} e^{-[2\pi \rho_{\min} \Delta\omega]^2 n^2} \right] \\ &= O\left(\rho_{\max}^{2d} \left[\Delta\omega + \Delta\omega \sum_{n=1}^{\infty} e^{-[2\pi \rho_{\min} \Delta\omega]^2 n^2} \right]^{d-1} \left[\Delta\omega \sum_{n=M+1}^{\infty} e^{-[2\pi \rho_{\min} \Delta\omega]^2 n^2} \right] \right) \\ &= O\left(\rho_{\max}^{2d} \left[\Delta\omega + \int_0^\infty e^{-[2\pi \rho_{\min} u]^2} du \right]^{d-1} \left[\int_{M\Delta\omega}^\infty e^{-[2\pi \rho_{\min} u]^2} du \right] \right) \\ &= O\left(\rho_{\max}^{2d} \rho_{\min}^{-d} e^{-[2\pi \rho_{\min} M \Delta\omega]^2} \right), \end{aligned}$$

assuming $\Delta\omega = O(1)$ and using the fact [11] that $\int_v^\infty e^{-x^2} dx = O(e^{-v^2})$.

assuming that $\Delta\omega = O(1)$.

Now to bound the first term on the right-hand side of (E.18), we use the Poisson summation formula, which implies that

$$(\Delta\omega)^d \sum_{\mathbf{n} \in \mathbb{Z}^d} \hat{f}(\mathbf{n}\Delta\omega) = \sum_{\mathbf{n} \in \mathbb{Z}^d} f(\mathbf{n}/\Delta\omega), \quad (\text{E.21})$$

where $f := \mathcal{F}^* \hat{f}$ is the inverse Fourier transform of \hat{f} , which can be calculated explicitly as

$$f(z) = \left(\frac{2\pi\sigma_k^2\sigma_l^2}{\sigma_k^2 + \sigma_l^2} \chi^2(t) \right)^{d/2} e^{-\frac{|z-(y-x)|^2}{2([\sigma_k\chi(t)]^2 + [\sigma_l\chi(t)]^2)}}. \quad (\text{E.22})$$

Note moreover that $\int_{\mathbb{R}^d} \hat{f}(\omega) d\omega = f(0)$, so from (E.21) it follows that

$$I_1 = \left| \sum_{\mathbf{n} \in \mathbb{Z}^d \setminus \{0\}} f(\mathbf{n}/\Delta\omega) \right| \leq \sum_{\mathbf{n} \in \mathbb{Z}^d \setminus \{0\}} |f(\mathbf{n}/\Delta\omega)|. \quad (\text{E.23})$$

Now from the expression (E.22) for f we deduce that

$$|f(z)| = O\left(\rho_{\max}^d e^{-\frac{|z-(y-x)|^2}{4\rho_{\max}^2}}\right), \quad (\text{E.24})$$

using the fact³ that $\frac{\sigma_k^2\sigma_l^2}{\sigma_k^2 + \sigma_l^2} \leq \frac{\sigma_{\max}^2}{2}$.

Then recall that we assume $x, y \in [-1, 1]^d$, so in turn it must be the case that $y - x \in [-2, 2]^d$. Therefore from (E.24) and the reverse triangle inequality we have that

$$|f(z)| = O\left(\rho_{\max}^d e^{-\frac{\sum_{i=1}^d [|z_i| - 2]_+^2}{4\rho_{\max}^2}}\right), \quad (\text{E.25})$$

from which it follows⁴ that I_1 can be bounded as

$$I_1 = O\left(\rho_{\max}^d e^{-\left[\frac{1}{4\rho_{\max}\Delta\omega}\right]^2}\right),$$

provided that $\Delta\omega \leq 1/8$. Combining with (E.20) in (E.18) completes the proof. \square

³This fact in turn follows from the identity $\frac{\sigma_k^2\sigma_l^2}{\sigma_k^2 + \sigma_l^2} = \frac{\sigma_k^2}{\sigma_k^2/\sigma_l^2 + 1} \leq \frac{\sigma_k^2}{2}$, which holds when $\sigma_k \geq \sigma_l$, together with similar reasoning in the opposite case.

⁴From (E.23) and (E.25) we can bound $I_1 \leq C\rho_{\max}^d \sum_{\mathbf{n} \in \mathbb{Z}^d \setminus \{0\}} e^{-\sum_{i=1}^d \left[\frac{n_i - 2\Delta\omega}{2\rho_{\max}\Delta\omega}\right]_+^2}$, for a suitable constant $C > 0$. Then again we can bound the sum over $\mathbb{Z}^d \setminus \{0\}$ with the sum of the sums over each of the ‘slab complements’ $\{\mathbf{n} : n_i \neq 0\}$ for $i = 1, \dots, d$, which are all equal, yielding:

$$\begin{aligned} I_1 &\leq C d \rho_{\max}^d \left[\sum_{n \in \mathbb{Z}} e^{-\left[\frac{n-2\Delta\omega}{2\rho_{\max}\Delta\omega}\right]_+^2} \right]^{d-1} \left[\sum_{n \in \mathbb{Z} \setminus \{0\}} e^{-\left[\frac{n-2\Delta\omega}{2\rho_{\max}\Delta\omega}\right]_+^2} \right] \\ &= O\left(\rho_{\max}^d \left[1 + \sum_{n=1}^{\infty} e^{-\left[\frac{n-2\Delta\omega}{2\rho_{\max}\Delta\omega}\right]_+^2} \right]^{d-1} \left[\sum_{n=1}^{\infty} e^{-\left[\frac{n-2\Delta\omega}{2\rho_{\max}\Delta\omega}\right]_+^2} \right]\right). \end{aligned}$$

Proof of Lemma 13. We employ definition 3.18 to write

$$\begin{aligned}
A &:= \|(\Delta\omega)^d \mathcal{B}_t^{(N_\sigma)} \mathcal{F}^* \Pi^* \Pi \mathcal{F} \mathcal{B}_t^{(N_\sigma)*} - \mathcal{B}_t^{(N_\sigma)} \mathcal{B}_t^{(N_\sigma)*}\| \\
&= \left\| (\Delta\omega)^d \left(\sum_{k=0}^{N_\sigma} \mathcal{W}_k \mathcal{G}_{k,t} \right) \mathcal{F}^* \Pi^* \Pi \mathcal{F} \left(\sum_{k=0}^{N_\sigma} \mathcal{G}_{k,t} \mathcal{W}_k \right) - \left(\sum_{k=0}^{N_\sigma} \mathcal{W}_k \mathcal{G}_{k,t} \right) \left(\sum_{k=0}^{N_\sigma} \mathcal{G}_{k,t} \mathcal{W}_k \right) \right\| \\
&\leq \sum_{k,l=0}^{N_\sigma} \left\| \mathcal{W}_k \left[(\Delta\omega)^d \mathcal{G}_{k,t} \mathcal{F}^* \Pi^* \Pi \mathcal{F} \mathcal{G}_{l,t} - \mathcal{G}_{k,t} \mathcal{G}_{l,t} \right] \mathcal{W}_l \right\|.
\end{aligned}$$

We want to continue our calculations to derive a suitable bound on A .

Now recall from 3.17 that \mathcal{W}_k as a pointwise multiplier by the function

$$w_k(x) := w(x) [2\pi \sigma^2(x)]^{-d/2} P_k(\sigma(x)). \quad (\text{E.26})$$

Therefore it follows from the preceding inequality that

$$A \leq \sum_{k,l=0}^{N_\sigma} \|w_k\|_\infty \|w_l\|_\infty \left\| (\Delta\omega)^d \mathcal{G}_{k,t} \mathcal{F}^* \Pi^* \Pi \mathcal{F} \mathcal{G}_{l,t} - \mathcal{G}_{k,t} \mathcal{G}_{l,t} \right\|,$$

where $\|\cdot\|_\infty$ denotes the L^∞ norm on $[-1, 1]^d$. Then we can apply Lemma 11 to obtain

$$A = O \left(\rho_{\max}^d \epsilon_{\mathcal{F}} \left[\sum_{k=0}^{N_\sigma} \|w_k\|_\infty \right]^2 \right).$$

Now if $\Delta\omega \leq \frac{1}{8}$, then

$$\begin{aligned}
\sum_{n=1}^{\infty} e^{-\left[\frac{n-2\Delta\omega}{2\rho_{\max}\Delta\omega}\right]_+^2} &\leq \sum_{n=1}^{\infty} e^{-\left[\frac{n-1/4}{2\rho_{\max}\Delta\omega}\right]^2} \\
&\leq \sum_{n=4}^{\infty} e^{-\left[\frac{n/4-1/4}{2\rho_{\max}\Delta\omega}\right]^2} \leq 4 \int_{3/4}^{\infty} e^{-\left[\frac{u-1/4}{2\rho_{\max}\Delta\omega}\right]^2} du = 4 \int_{1/2}^{\infty} e^{-\left[\frac{u}{2\rho_{\max}\Delta\omega}\right]^2} du = O \left(e^{-\left[\frac{1}{4\rho_{\max}\Delta\omega}\right]^2} \right),
\end{aligned}$$

again using the fact that $\int_v^\infty e^{-x^2} dx = O(e^{-v^2})$.

Then

$$\begin{aligned}
I_1 &= O \left(\rho_{\max}^d \left[1 + \sum_{n=1}^{\infty} e^{-\left[\frac{n-2\Delta\omega}{2\rho_{\max}\Delta\omega}\right]_+^2} \right]^{d-1} \left[\sum_{n=1}^{\infty} e^{-\left[\frac{n-2\Delta\omega}{2\rho_{\max}\Delta\omega}\right]_+^2} \right] \right) \\
&= O \left(\rho_{\max}^d \left[1 + e^{-\left[\frac{1}{4\rho_{\max}\Delta\omega}\right]^2} \right]^{d-1} \left[e^{-\left[\frac{1}{4\rho_{\max}\Delta\omega}\right]^2} \right] \right) \\
&= O \left(\rho_{\max}^d 2^{d-1} e^{-\left[\frac{1}{4\rho_{\max}\Delta\omega}\right]^2} \right) \\
&= O \left(\rho_{\max}^d e^{-\left[\frac{1}{4\rho_{\max}\Delta\omega}\right]^2} \right)
\end{aligned}$$

since we treat d as constant.

It remains to bound $\|w_k\|_\infty$. Recall our assumption 5.1 ensuring that $\|w\|_\infty \leq 1$, and moreover recall that the Chebyshev interpolating functions P_k [10, Chapter 5] are bounded in magnitude by 1 on their domain $[\sigma_{\min}, \sigma_{\max}]$. Therefore from E.26 it follows that $\|w_k\|_\infty = O(\sigma_{\min}^{-d})$, and consequently

$$A = O(N_\sigma^2 \sigma_{\min}^{-2d} \rho_{\max}^d \epsilon_{\mathcal{F}}).$$

Since $\rho_{\max}/\sigma_{\min}^2 = \kappa \frac{\chi_{\max}}{\sigma_{\min}}$, we have completed the proof. \square

F Proof of Theorem 14

Proof of Theorem 14. We will focus first on the general Matérn case.

By the triangle inequality, we bound

$$\begin{aligned} \|\mathcal{K} - \tilde{\mathcal{K}}\| &\leq \left\| \mathcal{K} - \sum_{j=0}^{N_t} \mathcal{B}_{t_j} \mathcal{B}_{t_j}^* v_j \right\| \\ &+ \left\| \sum_{j=0}^{N_t} \mathcal{B}_{t_j} \mathcal{B}_{t_j}^* v_j - \sum_{j=0}^{N_t} \mathcal{B}_{t_j}^{(N_\sigma)} \mathcal{B}_{t_j}^{(N_\sigma)*} v_j \right\| \\ &+ \underbrace{\left\| \sum_{j=0}^{N_t} \mathcal{B}_{t_j}^{(N_\sigma)} \mathcal{B}_{t_j}^{(N_\sigma)*} v_j - (\Delta\omega)^d \sum_{j=0}^{N_t} \mathcal{B}_{t_j}^{(N_\sigma)} \mathcal{F}^* \Pi^* \Pi \mathcal{F} \mathcal{B}_{t_j}^{(N_\sigma)*} v_j \right\|}_{\tilde{\mathcal{K}}}. \end{aligned}$$

The bound is justified because the underbraced expression is precisely $\tilde{\mathcal{K}}$, following (3.19). Let the three terms on the right-hand side be denoted T_1 , T_2 , and T_3 , respectively.

First we cite Lemma 4, which establishes that

$$T_1 = O(\sigma_{\min}^{-d} \epsilon_{\text{trap}}). \quad (\text{F.1})$$

Then we bound, using 10:

$$T_2 \leq \sum_{j=0}^{N_t} |v_j| \left\| \mathcal{B}_{t_j} \mathcal{B}_{t_j}^* - \mathcal{B}_{t_j}^{(N_\sigma)} \mathcal{B}_{t_j}^{(N_\sigma)*} \right\| = O\left(\Lambda_{N_\sigma} \rho_{\max}^d \epsilon_{\text{cheb}} \sum_{j=0}^{N_t} |v_j|\right).$$

Now $|v_j| \leq v(t_j) \Delta t$, and moreover $v(t) = \chi^{-d}(t) u(t) = O(e^{(\nu - \frac{d}{2})t - e^t})$. Thus ν is integrable, and $\sum_{j=0}^{N_t} |v_j| = O(1)$. It follows that

$$T_2 = O(\Lambda_{N_\sigma} \rho_{\max}^d \epsilon_{\text{cheb}}). \quad (\text{F.2})$$

Finally, using Lemma 13, we bound:

$$T_3 \leq \sum_{j=0}^{N_t} |v_j| \left\| \mathcal{B}_{t_j}^{(N_\sigma)} \mathcal{B}_{t_j}^{(N_\sigma)*} - (\Delta\omega)^d \sum_{j=0}^{N_t} \mathcal{B}_{t_j}^{(N_\sigma)} \mathcal{F}^* \Pi^* \Pi \mathcal{F} \mathcal{B}_{t_j}^{(N_\sigma)*} \right\|$$

$$= O \left(N_\sigma^2 \kappa^d \left[\frac{\chi_{\max}}{\sigma_{\min}} \right]^d \epsilon_{\mathcal{F}} \sum_{j=0}^{N_t} |v_j| \right).$$

Again using the fact that $\sum_{j=0}^{N_t} |v_j| = O(1)$, we conclude that

$$T_3 = O \left(N_\sigma^2 \kappa^d \left[\frac{\chi_{\max}}{\sigma_{\min}} \right]^d \epsilon_{\mathcal{F}} \right). \quad (\text{F.3})$$

Combining (F.1), (F.2), and (F.3), we conclude that

$$\|\mathcal{K} - \tilde{\mathcal{K}}\| = O \left(\sigma_{\min}^{-d} \epsilon_{\text{trap}} + \Lambda_{N_\sigma} \rho_{\max}^d \epsilon_{\text{cheb}} + N_\sigma^2 \kappa^d \left[\frac{\chi_{\max}}{\sigma_{\min}} \right]^d \epsilon_{\mathcal{F}} \right),$$

as was to be shown.

The logic in the case of the squared-exponential kernel is exactly the same, except that there is no integration over t and so the first error term (T_1) is discarded. \square